

The influences of the Magellanic Clouds on the Galaxy: Pole shift, warp, and star formation history

Kenji Bekki^{1*}

¹*ICRAR M468 The University of Western Australia 35 Stirling Hwy, Crawley Western Australia, 6009*

Accepted, Received 2005 February 20; in original form

ABSTRACT

We investigate how the Large Magellanic Cloud (LMC) influences the evolution of the Galaxy after the LMC enters into the virial radius of the dark matter halo of the Galaxy for the first time. Both the Galaxy and the LMC are modeled as N-body particles in our models so that the dynamical influences of the LMC on the Galaxy can be investigated in a fully self-consistent manner. Furthermore, the orbital parameters for the LMC are carefully chosen such that the present location of the LMC in the Galaxy can be rather precisely reproduced in our simulations. We particularly investigate the influences of the LMC on the precession rate, the outer stellar and gaseous structures, and the star formation history of the Galaxy. Our principal results are summarized as follows. The LMC-Galaxy dynamical interaction can cause “pole shift” (or irregular precession/nutation) of the Galaxy and the typical rate of pole shift ($\dot{\theta}_d$) is ~ 2 degree Gyr^{-1} corresponding to $\sim 7\mu\text{as yr}^{-1}$. The LMC-Galaxy interaction induces the formation of the outer warp structures of the Galaxy, which thus confirms the results of previous numerical simulations on the formation of the Galactic warp. The LMC-Galaxy interaction also induces the formation of outer ($R > 20$ kpc) spiral arms and increases the vertical velocity dispersion of the outer disk significantly. The mean star formation rate of the Galaxy for the last several Gyrs can be hardly influenced by the LMC’s tidal force. The age and metallicity distribution of stars in the solar-neighborhood ($7 \text{ kpc} \leq R \leq 10 \text{ kpc}$) for the last several Gyr can be only slightly changed by the past LMC-Galaxy interaction. If the LMC is accreted onto the Galaxy as a group with small dwarf galaxies, then the stripped dwarfs form a unique polar distribution within the Galaxy. Based on these results, we discuss how the possible ongoing Galactic pole shift with $\dot{\theta}_d \sim 10 \mu\text{as yr}^{-1}$ can be detected by future observational studies by GAIA.

Key words: Magellanic Clouds – galaxies:structure – galaxies:kinematics and dynamics – galaxies:halos

1 INTRODUCTION

The tidal field of the Galaxy and the hydrodynamical influences of the warm gaseous halo have long been considered to be key ingredients in the evolution of the LMC and the Small Magellanic Cloud (SMC). The strong gravitational field of the massive dark matter halo of the Galaxy can influence not only the dynamical evolution of the LMC (e.g., Gardiner et al. 1994) but also its long-term star formation history (Bekki & Chiba 2005; BC05). The hydrodynamical interaction between the Galactic halo and cold interstellar medium (ISM) of the LMC can be responsible for the stripping of ISM from the LMC (e.g., Mastropietro et al. 2005; M05). The strong

tidal field of the Galaxy can play a vital role in the formation of the bifurcated structures of the Magellanic Stream and its elongated leading arm features (e.g., Gardiner & Noguchi 1996, GN96; Yoshizawa & Noguchi 2003, YN03; Connors et al. 2006; Diaz & Bekki 2011a, b, c, DB11a, b, and c, respectively). The orbital evolution of the LMC and the SMC, which is essentially important for the evolution of the Clouds, strongly depend on the mass model of the Galaxy and the present day proper motions of the Clouds (e.g., Lin & Lynden-Bell 1977; Murai & Fujimoto 1980; Kallivayalil et al. 2006; Besla et al. 2007, B07; Ruzicka et al. 2010).

Although previous theoretical studies clarified the important influences of the LMC-Galaxy interaction on the evolution of the LMC (e.g., BC05; M05), they did not discuss how the LMC-Galaxy interaction influences the evolution of the Galaxy. Furthermore the influences of the LMC

* E-mail: bekki@cyllene.uwa.edu.au

on the Galaxy have been so far discussed only in the context of the formation processes of the Galactic warps (e.g., Hunter & Toomre 1969; Weinberg 1998; Tsuchiya 2002). Previous observations on the long-term star formation history in the solar-neighborhood suggested that the star formation history (in particular, a number of possible bursts of star formation) might have been influenced by the LMC-Galaxy tidal interaction (e.g., Rocha-Pinto et al. 2000). The possible influences of the LMC on the Galactic star formation history, however, have not been discussed so far by theoretical studies based on numerical simulations. The previous numerical simulations on the Galactic warp formation did not consider the latest observational results on the proper motions of the LMC and the SMC (e.g., Costa et al. 2009; Vieira et al. 2010). Thus more self-consistent numerical simulations are necessary to address a number of key questions related to the Galaxy evolution influenced by the LMC.

The purpose of this paper is thus to investigate the influences of the LMC-Galaxy interaction on the evolution of the Galaxy using more realistic and more self-consistent numerical simulations. The present study is significantly improved over the previous theoretical studies as follows. First, the Galaxy is modeled as a three-component system (bulge, disk, and dark matter halo) represented by N-body particles so that both dynamical friction of the LMC against the Galactic halo and the structural and kinematical changes of the Galactic halo due to the LMC-Galaxy interaction can be self-consistently investigated. Second, not only the orbital evolution of the LMC since its first infall onto the Galaxy from outside the virial radius but also the mass evolution (e.g., mass loss) of the LMC are investigated so that the long-term influences of the LMC on the Galaxy can be quantitatively estimated. Furthermore, star formation processes and gas dynamics in the Galaxy are included in some models of the present study (though they are idealized in some points) so that the influences of the LMC on the Galactic star formation history can be investigated.

We consider that one of the important influences of the LMC on the Galaxy is the induction of the Galactic precession/nutation (or “pole shift”) in the present study. As discussed later in this paper, if the precession of the Galaxy is really ongoing, it has a number of potentially important implications in the modern astronomy. Thus it is doubtless worthwhile for the present study to predict the possible direction and rate of the Galactic precession/nutation/pole-shift ($\dot{\theta}_d$) caused by the past LMC-Galaxy interaction and thereby discuss whether the precession/nutation/pole-shift can be detected by future observational studies by GAIA and VLBI.

It is essential for the present study to reproduce rather precisely the present location of the LMC with respect to the Galactic center, because we discuss the present structure and kinematics of the Galaxy influenced by the LMC. Previous studies on the past orbital evolution of the LMC (e.g., MF80; YN03) are based on the “backward integration scheme” in which the past orbit of the LMC can be readily investigated for given present three dimensional (3D) position and velocity of the LMC. In the present study, we do not adopt the backward integration scheme but instead investigate the orbital evolution of the LMC from the past to the present by using N-body simulations. Therefore, we need to run at least a number of models with different initial

locations and velocities of the LMC in order to find a model which can reproduce the present location of the LMC. It is accordingly numerically costly for the present study to find a model that reproduces well the present location of the LMC. But the present numerical simulations need to be done to properly investigate the influences of the Magellanic Clouds on the Galaxy evolution.

The layout of this paper is as follows. In §2, we summarize our numerical models for the LMC-Galaxy interaction and describe the method to find a model that reproduces the present location of the LMC. We present the results of the collisionless simulations on the Galactic structure and kinematics influenced by the LMC in §3. In §4, we briefly discuss how the Galactic star formation history can be influenced by the LMC-Galaxy interaction using models with gas dynamics and star formation. In this section, we also present some important implications of the present numerical results in the long-term evolution of the Galaxy. The conclusions of the present study are given in §5.

2 THE COLLISIONLESS MODEL

2.1 The Galaxy

Since the present model of the Galaxy is essentially the same as that adopted in our previous study on the dynamical evolution of disk galaxies (Bekki & Peng 2006), we here briefly describe the model. A much larger number of particles ($> 10^6$) are used for a galaxy in the present study (in comparison with our previous work above) so that we can discuss evolution of global disk structures under the influences of weaker tidal perturbation. The total mass and the virial radius of the dark matter halo of the galaxy are denoted as $M_{\text{dm,mw}}$ and $r_{\text{vir,mw}}$, respectively. We adopted an NFW halo density distribution (Navarro, Frenk & White 1996) suggested from CDM simulations:

$$\rho(r) = \frac{\rho_0}{(r/r_s)(1+r/r_s)^2}, \quad (1)$$

where r , ρ_0 , and r_s are the spherical radius, the characteristic density of a dark halo, and the scale length of the halo, respectively. We adopted $c = 10$ ($= r_{\text{vir,mw}}/r_s$) and $r_{\text{vir,mw}} = 245$ kpc, and the mass ratio of halo to disk was fixed at 16.7 ($M_{\text{dm,mw}} = 10^{12} M_\odot$ for the adopted disk mass). The adopted total mass of the Galaxy is consistent with the observationally estimated value of $1.9^{+3.6}_{-1.7} \times 10^{12} M_\odot$ (Wilkinson & Evans 1999).

The stellar disk with the size R_d and the mass M_d is assumed to have an exponential profile with the radial and vertical scale lengths of 3.5 kpc and 0.35 kpc, respectively. The stellar disk is assumed to have $M_d = 6 \times 10^{10} M_\odot$, $R_d = 17.5$ kpc, the Toomre Q-parameter of 1.5, and the maximum circular velocity of ~ 220 km s $^{-1}$. The bulge is represented by a Hernquist bulge and has a mass of $10^{10} M_\odot$ and a size of 3.5 kpc (scale-length of 700 pc). The disk galaxy is assumed to have no gas and no star formation. The initial disk plane of the galaxy is set to be the x - y plane in the present study (i.e., the z -axis is the polar direction of the galaxy). Fig. 1 shows the radial profile of the circular velocity (V_c) of the present disk model.

Recent observational studies have revealed the detailed structural properties of the outer stellar and gaseous disks of

Table 1. Description of the model parameters for the representative models.

Model	$M_{\text{dm,mw}}^a$	$r_{\text{vir,mw}}^b$	$M_{\text{dm,l}}^c$	R_{edc}^d	f_v^e	$f_{v,t}^f$	$f_{v,r}^g$	Dwarfs ^h	comments
T1	10^{12}	245	9×10^{10}	35	0.63	0.6	0.2	No	the standard model
T2	10^{12}	245	9×10^{10}	35	0.45	0.4	0.2	No	
T3	10^{12}	245	9×10^{10}	35	0.54	0.5	0.2	No	
T4	10^{12}	245	9×10^{10}	35	0.73	0.7	0.2	No	
T5	10^{12}	245	9×10^{10}	35	0.60	0.6	0.0	No	
T6	10^{12}	245	9×10^{10}	35	0.85	0.6	0.6	No	
T7	10^{12}	245	9×10^{10}	35	1.17	0.6	1.0	No	
T8	10^{12}	245	9×10^{10}	35	1.35	0.9	1.0	No	
T9	10^{12}	245	3×10^{10}	35	0.63	0.6	0.2	No	low-mass LMC
T10	10^{12}	245	6×10^{10}	35	0.63	0.6	0.2	No	high-mass LMC
T11	10^{12}	245	1.2×10^{11}	35	0.63	0.6	0.2	No	
T12	10^{12}	245	3×10^{10}	35	0.45	0.4	0.2	No	
T13	10^{12}	245	3×10^{10}	35	0.54	0.5	0.2	No	
T14	10^{12}	245	6×10^{10}	35	0.63	0.7	0.2	No	smaller EDC larger EDC first passage model
T16	10^{12}	245	9×10^{10}	25	0.63	0.6	0.2	No	
T17	10^{12}	245	9×10^{10}	45	0.63	0.6	0.2	No	
T18	10^{12}	245	9×10^{10}	35	1.12	0.5	1.0	No	
T19	10^{12}	245	3×10^{10}	35	1.12	0.5	1.0	No	
T20	10^{12}	245	1.2×10^{11}	35	1.12	0.5	1.0	No	
T21	5×10^{11}	245	3×10^{10}	35	0.63	0.6	0.2	No	low-mass Galaxy
T22	5×10^{11}	245	9×10^{10}	35	0.63	0.6	0.2	No	20 dwarfs, $R_{\text{dw}} = 10R_{\text{d,l}}$
T23	10^{12}	245	9×10^{10}	25	0.63	0.6	0.2	Yes	
T24	10^{12}	245	9×10^{10}	25	0.63	0.6	0.2	Yes	20 dwarfs, $R_{\text{dw}} = 5R_{\text{d,l}}$
I1	10^{12}	245	—	35	-	-	-	No	isolated model
I2	10^{12}	245	—	25	-	-	-	No	
I3	10^{12}	245	—	45	-	-	-	No	

^a The total dark halo mass of the Galaxy in units of M_{\odot} .^b The virial radius of the Galactic dark matter halo in units of kpc.^c The total dark halo mass of the LMC in units of M_{\odot} .^d The size of the extended disk component (EDC) in the Galaxy in units of kpc.^e The ratio of the velocity of the LMC (v_L) to the circular velocity (v_{cir}) at the initial position of the LMC.^f The initial tangential velocity of the LMC is given as $f_{v,t}v_{\text{cir}}$.^g The initial radial velocity of the LMC is given as $f_{v,r}v_{\text{cir}}$.^h Presence (“Yes”) or absence (“No”) of dwarf galaxies of the LMC group in the model.

the Galaxy (e.g., McClure-Griffiths, et al. 2004; Levine et al. 2006, 2007; Momany et al. 2006). In order to investigate the dynamical influences of the LMC on the outer part ($R > 20$ kpc) of the Galactic stellar and gaseous disks, we assume that the Galaxy has an extended disk component (referred to as “EDC” from now on for convenience). Although the present simulations are purely collisionless so that we can not investigate the LMC’s influences on the outer gas disk of the Galaxy, the inclusion of the EDC in the present simulations can help us to understand the LMC’s influences on the outer part of the Galaxy. The mass fraction of the EDC to the Galactic stellar disk is fixed at 0.1 (i.e., the EDC’s mass of $6 \times 10^9 M_{\odot}$) and the size (R_{edc}) is a free parameter ranging from 25 kpc to 45 kpc. The radial scale length of the EDC is set to be $0.5R_{\text{edc}}$ for all models whereas two different values for the vertical scale height ($0.0025R_{\text{edc}}$ and $0.01R_{\text{edc}}$) are adopted.

The total numbers of particles used for dark matter halo, stellar disk, bulge, and EDC of a disk galaxy in a simulation are 800000, 200000, 33400, and 50000, respectively. This simulation with these particle numbers is referred to as a “high-resolution” simulation for convenience, just because the particle numbers are larger than those used in “low-resolution simulations later described. The adopted gravitational softening length is fixed at 200pc for all components

(e.g., dark matter halo and disk) in all high-resolution models. We investigate some models with the total particle number of EDC being 200000 in order to confirm that the present results (in particular, the formation of the Galactic warp) do not depend on the resolution of the simulations. Table 2 briefly summarizes the particle mass and the total particle number of each component used in the present simulations.

We investigate models in which the Galaxy is not influenced by the LMC at all and they are referred to as “isolated models” (e.g., I1). In order to confirm that the central bar of the Galaxy can be formed in the isolated model, we investigate the dynamical evolution of the isolated model. Fig. 2 shows the final two-dimensional (2D) distribution of disk stars projected onto the x - y plane after 5.2 Gyr dynamical evolution of the isolated Galaxy model (I1). The 2D surface mass density (μ_s) is given in logarithmic scale in this figure and all other figures on the 2D distributions of stars. The disk clearly has a central bar/box bulge, which is consistent with the observed Galaxy. It should be noted here that the global stellar bar of the Galaxy can be formed *spontaneously* as a result of bar instability without tidal interaction with the LMC. It is confirmed that the EDC does not show any warps in the final disk for this isolated model.

The mass of the Galaxy at the epoch of the LMC accretion could be significantly smaller than the present mass of

the Galaxy owing to the continuous growth via accretion of gas, dark matter, and small galaxies. We therefore investigate the “low-mass” model for the Galaxy in which $M_{\text{dm,mw}}$ and $r_{\text{vir,mw}}$ are $5 \times 10^{11} M_{\odot}$ and 206 kpc, respectively. The Galaxy can be more strongly influenced by the LMC for a given mass of the LMC in this low-mass Galaxy model. The total mass of the Galaxy is fixed for all models in the present study. It is our future study to investigate the orbital evolution of the LMC in the time-changing gravitational potential due to the mass growth of the Galaxy.

2.2 The LMC

The LMC is assumed to be accreted onto the Galaxy from outside the virial radius of the dark matter halo ($R > 245$ kpc). Therefore, the LMC has a dark matter halo that is not tidally truncated and thus can have a total mass much larger than that of the present dark matter halo of the LMC ($\sim 10^{10} M_{\odot}$). The dark matter halo of the LMC is assumed to have the NFW profile with $c = 12$, and the total mass of the halo ($M_{\text{dm,l}}$) within the virial radius ($r_{\text{vir,l}}$) is a free parameter that controls the orbital evolution of the LMC. The LMC is assumed to be a bulge-less dwarf disk galaxy with the disk mass $M_{\text{d,l}}$ and the disk size $R_{\text{d,l}}$. The mass-ratio of the disk to the halo is fixed at 16.7 for all models in the present study. The LMC has an exponential disk with the scale length and vertical scale-height are fixed at $0.2R_{\text{d,l}}$ and $0.02R_{\text{d,l}}$, respectively. The Toomre Q -parameter of the disk is set to be 1.5 for all models.

We mainly investigate the LMC models with $M_{\text{dm,l}} = 9 \times 10^{10} M_{\odot}$, $M_{\text{d,l}} = 5.4 \times 10^9 M_{\odot}$, and $r_{\text{vir,l}} = 74.9$ kpc. This model shows the maximum circular velocity ($v_{\text{max,l}}$) of $\sim 110 \text{ km s}^{-1}$, which is consistent with some observational results (e.g., Olsen & Massey 2007; Piatek et al. 2008). We however investigate models with different $M_{\text{dm,l}}$, because observational studies of $v_{\text{max,l}}$ derived from kinematic of different stellar populations show different results (e.g., Olsen & Massey 2007). As suggested by our previous study (Bekki 2008), the LMC was accreted onto the Galaxy as a group with some satellite dwarf galaxies. Other faint group member galaxies are not distributed within the LMC halo from most models in the present study, because they can not be so important in the orbital evolution of the LMC (group) owing to the much smaller total mass of the dwarfs in comparison with the dark matter of the LMC.

We however investigate several models with 20 small dwarfs in order to discuss the present distribution of the stripped dwarfs in the outer region of the Galactic halo. The masses of the 20 dwarfs are assumed to be the same ($0.001M_{\text{d,l}}$ for each) and they are distributed within a radius of R_{dw} . The radial number distribution of the dwarfs is assumed to follow the power-law profile with the power-law index of -3.5 and the scale length of the profile of $0.5R_{\text{dw}}$. We investigate models with different R_{dw} so that we can discuss how the present distribution of the stripped dwarfs depends on the initial distribution of the dwarfs in the LMC. The results are discussed in §4.

Here we do not include the influences of the SMC on the orbit of the LMC for the following two reasons. The first one is that the present mass of the SMC ($\sim 3 \times 10^9 M_{\odot}$) is significantly smaller than that of the LMC ($2 \times 10^{10} M_{\odot}$; GN96); this means that the present mass of the SMC is much

Table 2. The particle mass and the total particle number of each component adopted for the standard model.

Component	Mass	Number
The Galaxy		
Dark matter	$1.3 \times 10^6 M_{\odot}$	800000
Stellar disk	$2.9 \times 10^5 M_{\odot}$	200000
Bulge	$2.9 \times 10^5 M_{\odot}$	33400
Extended disk	$1.2 \times 10^5 M_{\odot}$	50000
LMC		
Dark matter	$9.0 \times 10^5 M_{\odot}$	100000
Stellar disk	$5.4 \times 10^4 M_{\odot}$	100000

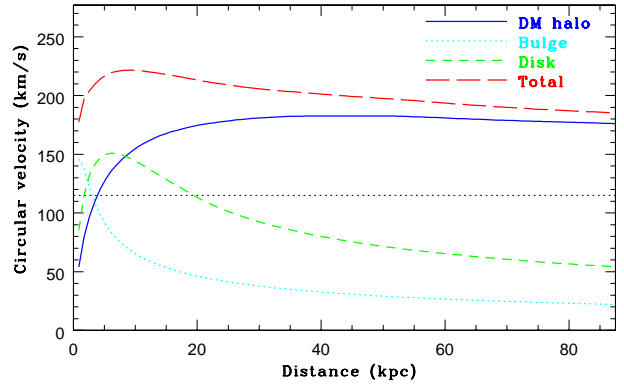


Figure 1. The rotation curve profile as a function of radius in the Galaxy for the standard model (red long-dashed line). Contributions of the dark halo, stellar bulge, and stellar disk are shown by blue solid line, cyan dotted one, and green short-dashed one, respectively. The black dotted line represents the maximum circular velocity of the LMC with $M_{\text{dm,l}} = 9 \times 10^{10} M_{\odot}$ in the standard model.

smaller than the original mass of the LMC ($\sim 10^{11} M_{\odot}$). The second is that we do not intend to discuss the formation of the Magellanic Stream from the tidal stripping of the gas initially in the SMC. We consider that the inclusion of the SMC can hardly change the present results on the influences of the LMC on the dynamical evolution and the star formation history of the Galaxy. Brief discussion of the orbital evolution of the LMC and the SMC in a live Galactic potential is given in Bekki (2011).

2.3 Simulation setup

Numerical computations were carried out both on (i) the latest version of GRAPE (GRAVity PipE, GRAPE-DR) – which is the special-purpose computer for gravitational dynamics (Sugimoto et al. 1990) and (ii) five high-end PCs and servers (e.g., one IBM system iDataPlex) with one or two GPU cards (Tesla M2050 and GTX580) and CUDA G5/G6 software package being installed for calculations of gravitational dynamics at University of Western Australia. We adopt a direct summation method for the calculation of gravitational force of each individual particle. It takes about 23 CPU hours for a GRAPE-DR machine to finish a high-resolution simulation for 8.4 Gyr evolution (corresponding to 3000 time steps with 2.8×10^6 yr time interval) of the LMC-Galaxy system. Although the calculation speed for a

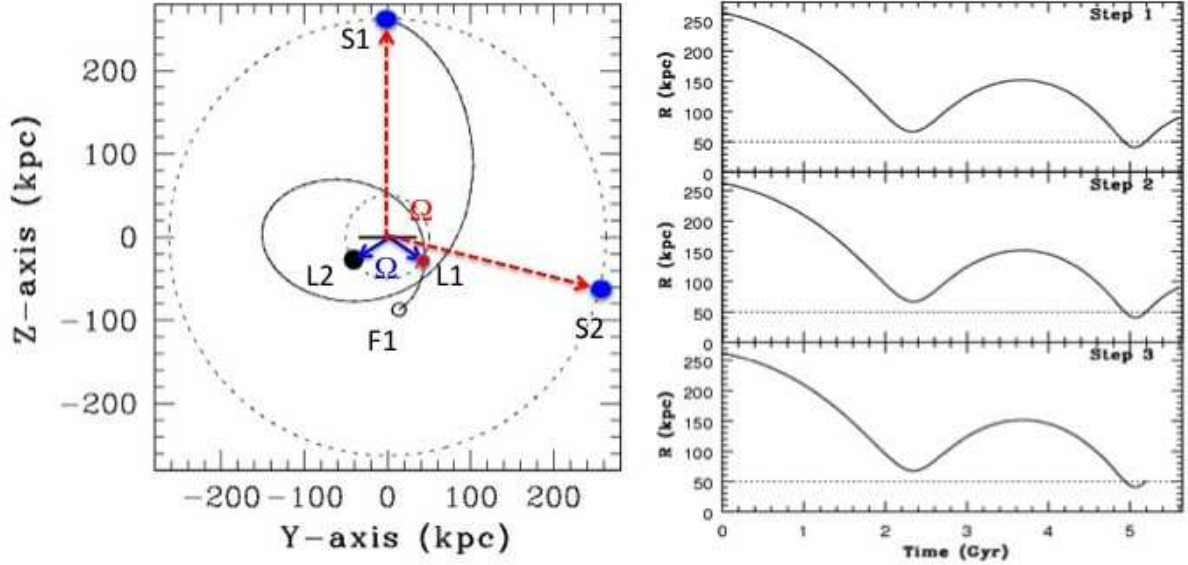


Figure 3. An illustrative figure for the new coordinate transformation method (CTM) by which we can reproduce the present location of the LMC rather precisely for a given set of orbital parameters of the LMC. In the left panel, the initial and final location of the LMC in the high-resolution simulation at Step 1 of the CTM are shown by a filled blue circle (S1) and a open circle (F1), respectively. The observed location of the LMC is shown by a filled black circle (L2) and the location L1 describes the point where the simulated LMC reaches $R = 50$ kpc for the second time in the simulation at Step 1. The angular distance between L1 and L2 is denoted as Ω and should be the same as that between S1 and S2, where S2 is the initial location of the LMC in the simulations at Step 2 and Step 3. The virial radius of the Galaxy and the present distance of the LMC from the Galaxy are shown by large and small dotted lines, respectively, in the left panel. In the right panel, the orbital evolution of the LMC is shown for the three simulations at Step 1 (top), Step 2 (middle), and Step 3 (bottom). The present distance of the LMC is shown by a dotted line in this panel. The details of the CTM are given in the main text.

simulation carried out by a GPU machine is significantly slower than that by the GRAPE, the five GPU machines enable us to investigate a parameter space for the LMC orbit in a quite efficient and productive way.

2.4 A new method to find an orbital model that reproduces the present LMC position

The present study adopts the new “coordinate transformation method (CTM)” rather than the backward integration scheme adopted by many previous studies (e.g., MF80; GN96; BC05; B07; DB11a, b, c) so that we can (i) investigate both the mass loss of the LMC and the dynamical friction of the LMC self-consistently and (ii) reproduce the present location of the LMC rather precisely. The present positions of the sun and the LMC are $(-8.5, 0, 0)$ kpc and $(-1.0, -40.8, -26.8)$ kpc, respectively (e.g., GN96; BC05). The sun is currently moving to the direction of the positive y in the coordinate system of the present study. This means that the Galaxy is rotating clockwise if it is viewed from the north Galactic pole (GN96). The initial distance between the LMC and the Galaxy is a free parameter and described as R_i . For all models, $R_i = 15R_d$ ($> R_{vir}$) so that we can investigate the orbital evolution of the LMC from outside the virial radius of the Galaxy. The tangential and radial velocities of the LMC at $R = R_i$ are set to be $f_{v,t}v_{cir}$ and $f_{v,r}v_{cir}$, respectively, where v_{cir} is the circular velocity at R_i . The LMC has a velocity of $f_v v_{cir}$ at R_i , where $f_v = (f_{v,t}^2 + f_{v,r}^2)^{0.5}$.

In order to more clearly explain the CTM in Fig.3, we here consider that the orbital plane of the LMC is coincident

with the y - z plane and the LMC has the initial velocity of $(0, f_{v,t}v_{cir}, -f_{v,r}v_{cir})$ at R_i . Fig. 3 illustrates the CTM for the LMC’s orbital plane being the same as the y - z plane. We take the following four steps (Step 0, 1, 2, and 3) in the CTM to find an orbital model that can reproduce the present LMC position for a given set of model parameters.

2.4.1 Step0: Running low-resolution simulations

First, we run a number of low-resolution simulations for a given set of model parameters (e.g., $M_{dm,l}$, R_i , $f_{v,t}$, and $f_{v,r}$) in order to find how long it takes for the LMC to have $R = 50$ kpc for the *second* time. Here the present LMC is considered to be going away from the Galaxy after the last pericenter passage ($R < 50$ kpc) about 0.2 Gyr ago. The time when the simulation starts is set to be 0 whereas the time when the LMC passes the pericenter for the second time is referred to as T_{50} for convenience. The particle numbers for dark matter, disk, bulge, and EDC of the Galaxy, and dark matter and disk of the LMC in a low-resolution simulation are 200000, 50000, 8350, 20000, 10000, and 10000, respectively. Although the total particle number of the low-resolution simulation is ~ 300000 , this number is enough to estimate T_{50} . For models with smaller $M_{dm,l}$ and larger f_v , T_{50} can be quite long (> 8 Gyr).

2.4.2 Step1: Running high-resolution simulations

If T_{50} is determined, we run a high-resolution model with $N > 1000000$ for a time scale (T_f) significantly larger than

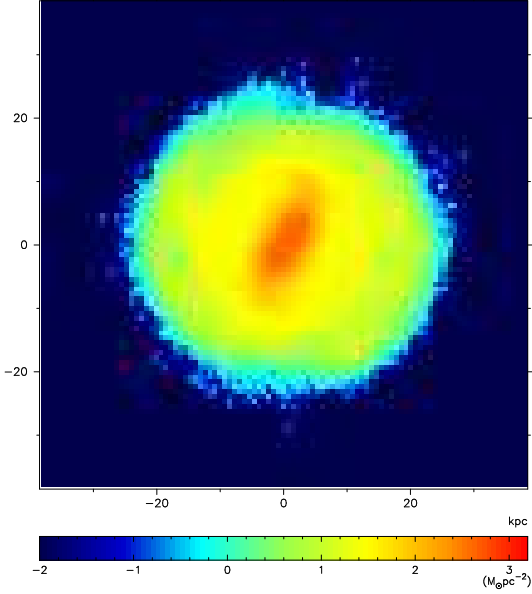


Figure 2. The 2D distribution of μ_s projected onto the x - y plane for disk stars of the Galaxy in the isolated model. Here μ_s is the smoothed surface mass density of stars in logarithmic scale (i.e., $\mu_s = \log_{10} \Sigma_s$, where Σ_s is the surface mass density of the stars). The 2D distribution is constructed based on the simulation data sets at $T = 5.2$ Gyr and the Gaussian smoothing of 875 pc.

Table 3. T_{50} and Ω for the representative four models estimated by using the new CTM.

Model	T_{50} ^a	Ω ^b
T1	5.2 Gyr	334°
T2	2.2 Gyr	241°
T3	2.3 Gyr	271°
T7	7.4 Gyr	5°

^a The time (T) when the LMC passes through the pericenter ($R < 50$ kpc) for the second time. The definition of this quantity is given in the main text.

^b The angular distance between the original and the transformed locations for the LMC position (at $T = 0$ in Figure 3). The definition of this quantity is given in the main text and in Figure 3.

T_{50} derived in the low-resolution one. This is mainly because even if the initial location of the LMC (“S1”) is the same between the low- and high-resolution simulations, the final location (“F1”) can be different between the two simulations. Thus we run a high-resolution simulation for T_f to ensure that the LMC can pass $R = 50$ kpc at least twice. The orbital evolution of the LMC in this high-resolution model is recorded for the following steps.

2.4.3 Step 2: Coordinate transformation

In this Step 2, we investigate the 3D position of the LMC (“L1” point in Fig. 3) in the Galactic coordinate when the LMC passes $R = 50$ kpc for the second time (T_{50}) in the high-resolution simulation. We compare the differences in the 3D position of the LMC between the simulation (“L1”) and the observation (“L2”) and thereby estimate the angu-

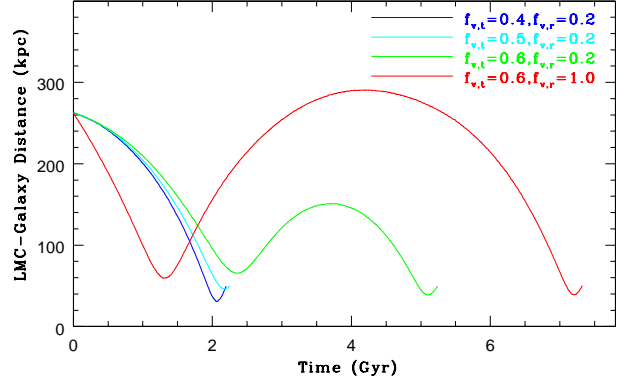


Figure 4. The orbital evolution of the LMC in the four representative models that can reproduce the present location of the LMC: $f_{v,t} = 0.4$ and $f_{v,r} = 0.2$ (blue), $f_{v,t} = 0.5$ and $f_{v,r} = 0.2$ (cyan), $f_{v,t} = 0.6$ and $f_{v,r} = 0.2$ (green), and $f_{v,t} = 0.6$ and $f_{v,r} = 1.0$ (red).

lar distance (Ω) between L1 and L2. We rotate the initial location of the LMC (“S1”) in the simulation by Ω so that the initial location of the LMC can be “S2”. We again run a high-resolution simulation with a new initial location of the LMC (S2) for T_f and thereby try to find when the LMC passes $R = 50$ kpc for the second time (T_{50}).

2.4.4 Step4: Rerunning simulations

If we can confirm whether the simulated LMC’s position at T_{50} can be almost identical to the observed location of the LMC, we rerun a high-resolution simulation (for the initial position S2) only for T_{50} and record the simulation data at the final time step ($T = T_{50}$) in order to analyze the data. The difference between the simulated and the observed locations ($\Delta r = (\Delta x^2 + \Delta y^2 + \Delta z^2)^{0.5}$) can be well less than ~ 2 kpc in the CTM. Thus, we have to run at least 4 simulations to have a model that can reproduce the present location of the LMC rather precisely for a given set of model parameters.

2.4.5 Advantages and disadvantages

The underlying assumption in the CTM is that the outer part of the Galaxy can be regarded as having an almost spherical mass distribution. Owing to the inclusion of a stellar disk in the present model, the Galactic potential is triaxial to some extent in the inner region of the Galaxy. However the CTM enables us to derive the LMC orbit model that can reproduce the present LMC position quite well, because both the apocenter and the pericenter of the LMC are significantly larger than the disk size of the Galaxy. Thanks to the CTM, we do not have to run a huge number of high-resolution simulations to find a model that reproduces the present LMC position quite well. This new CTM can be used for investigating the past orbital evolution of other dwarf galaxies in the Local Group. One of disadvantages of the CTM is that it can be difficult to reproduce the present location of the LMC for the case where the Galactic potential is triaxial to a significant extent. This weakness of the CTM needs to be improved in our future studies.

Also, although Δr can be rather small in the CTM,

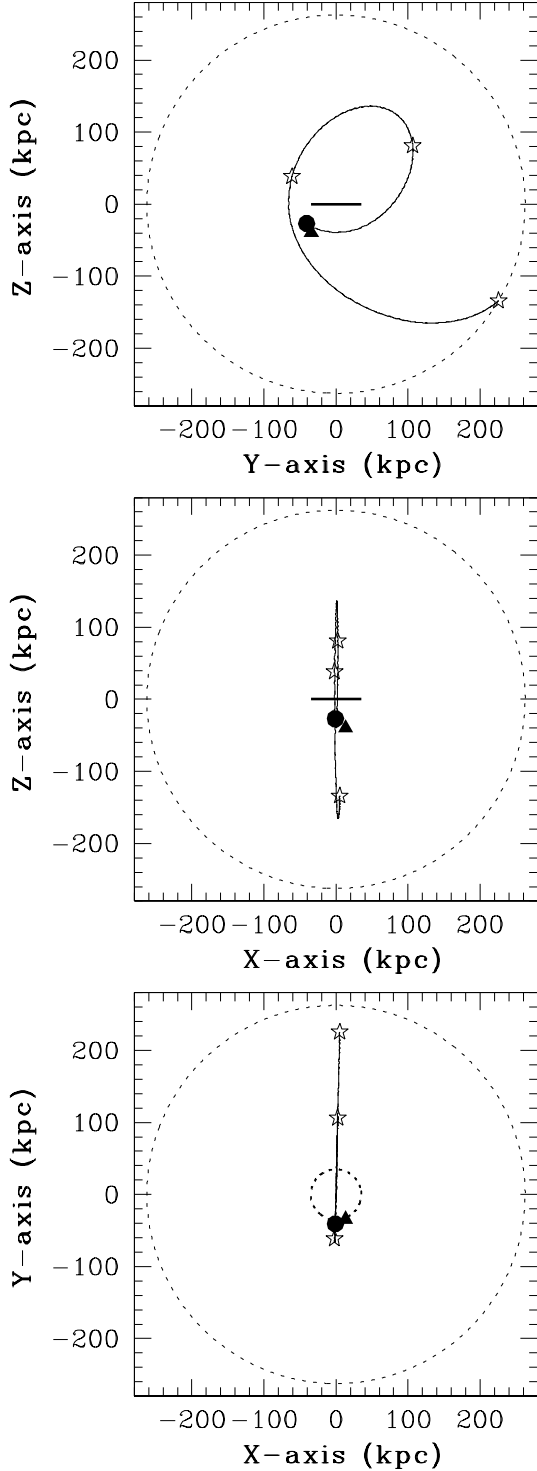


Figure 5. The orbital evolution of the LMC projected onto the y - z plane (top), the x - z one (middle), and the x - y one (bottom) in the standard model. The size of the EDC and the virial radius of the Galaxy are shown by a thick solid line and a thin dotted one, respectively. The size of the EDC is shown by a dotted line in the x - y projection so that the locations of the LMC and the SMC can be more clearly seen. The present locations of the LMC and the SMC are shown by a circle and a triangle, respectively. The locations of the simulated LMC at $T = -5.2$ Gyr, -2.7 Gyr, and -1.0 Gyr are shown by open stars.

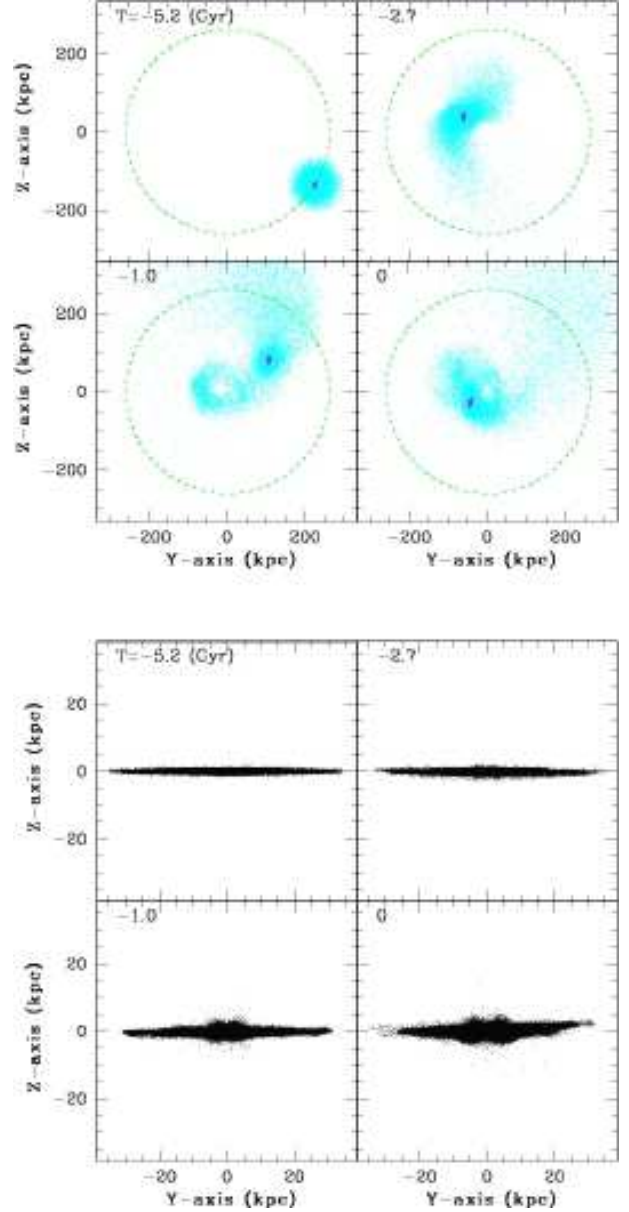


Figure 6. The evolution of the mass distribution projected onto the y - z plane for the LMC (upper four) and the EDC of the Galaxy (lower four) in the standard model. The disk and dark halo components of the LMC are shown by red and cyan particles, respectively, in the upper panel, and the dotted line represents the virial radius of the Galaxy. The time in the upper left corner of each panel is given in units of Gyr.

the velocity difference between the observed and simulated one ($\Delta v = (\Delta v_x^2 + \Delta v_y^2 + \Delta v_z^2)^{0.5}$) can not be so small. For example, Δv in the standard model (T1) is $\sim 80 \text{ km s}^{-1}$ (i.e., $\sim 40 \text{ km s}^{-1}$ in each velocity component). Other models show similar magnitudes of velocity differences (Δv). The difference in the proper motion of the LMC between different observations (e.g., Kallivayalil et al. 2006; Costa et al. 2009; Vieira et al. 2010), is not so small ($\sim 80 \text{ km s}^{-1}$) either. If future observations will more precisely determine the proper motion of the LMC (with an accuracy of less than 10 km s^{-1}), then the CTM needs to be improved significantly.

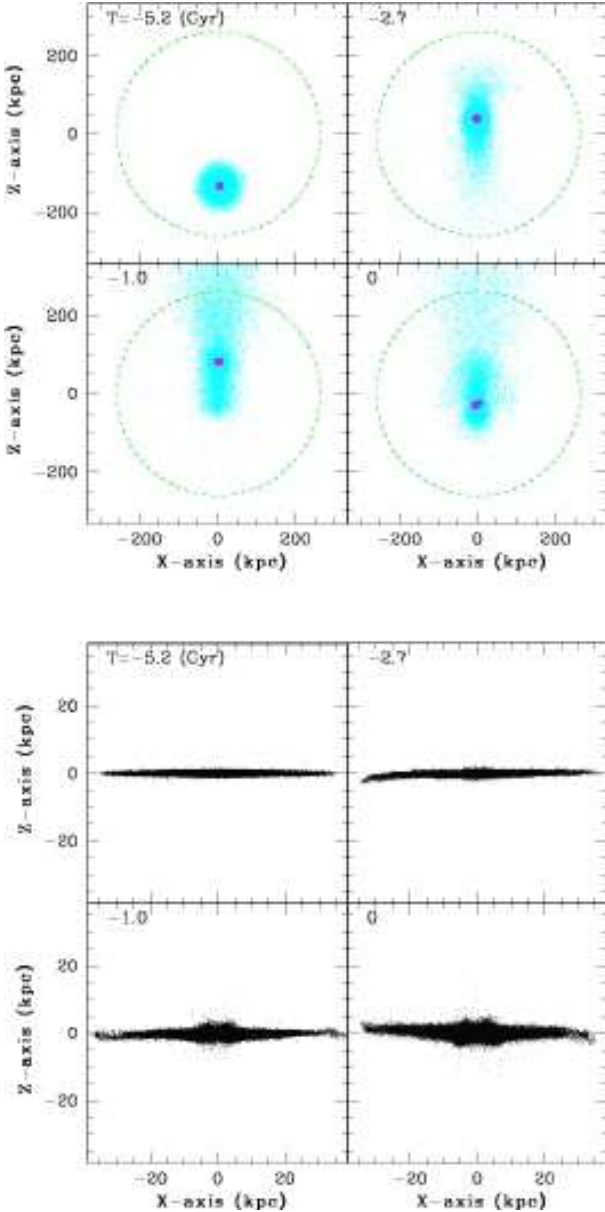


Figure 7. The same as Fig. 6 but for the x - z projection.

2.4.6 The orbital plane of the LMC

The orbital plane of the LMC is defined as a plane that is perpendicular both to the position vector of the LMC and the velocity one of the LMC. In the present study, we consider that the orbital plane of the LMC is similar to those used in successful models for the formation of the Magellanic Stream (e.g., GN96, DB11c): the best model by GN96 has the present LMC velocity of $(-5, -225, 194)$ km s $^{-1}$. Fig. 4 shows four examples of successful models (T1, T2, T3, and T7) in which the orbital planes are almost the same as that in GN96 and the present location of the LMC can be well reproduced. Table 3 summarizes T_{50} and Ω in the CTM for these four models. We also investigate some models in which the orbital plane of the LMC is the same as that adopted in DB11c, in which the present 3D velocity of the LMC is $(-51, -226, 229)$ km s $^{-1}$. We describe the results of the models with the best orbit in GN96, because the results of

the models with the two different orbital planes adopted by GN96 and DB11c are essentially similar.

2.5 Estimation of the Galactic precession/nutation/pole-shift

We investigate the time evolution of the rotation (i.e. angular momentum) vector $\mathbf{L}_d = (L_x, L_y, L_z)$ of the stellar disk for each model: this vector defines the orientation of the rotation axis of the stellar disk. We investigate (i) the inclination angle θ_d between the z -axis and the rotation vector of the disk galaxy and (ii) the angle ϕ_d between the rotation vector projected onto the x - y plane and the x -axis at selected time steps for each model. We estimate θ_d and ϕ_d as $\arccos(L_z/L_t)$ and $\arccos(L_x/L_{xy})$, respectively, where L_t is the absolute magnitude of the angular momentum and $L_{xy} = (L_x^2 + L_y^2)^{0.5}$. L_z is positive if the Galaxy rotates clock-wise viewed from the north Galactic pole. The rotation vector \mathbf{L}_d is estimated with respect to the central stellar particle that is initially located at the exact center of the disk and has no initial 3D velocities. However, these central particles later can be slightly dislocated from their initial central positions and have tiny 3D velocities due to the evolution of the disk. As a result of this, the time evolution of \mathbf{L}_d derived in some models can show rapid short-term increase and decrease with a small amplitude.

We also investigate the rate of precession/nutation/pole-shift of the Galaxy ($\dot{\theta}_d$) in order to provide predictions of the present θ_d of the Galaxy. The predicted $\dot{\theta}_d$ can be compared with the corresponding observations, if future observational studies based on GAIA and VLBI can detect the Galactic precession/nutation/pole-shift. Although $\dot{\theta}_d$ can become both negative and positive in its long-term evolution, $\dot{\theta}_d$ can keep its sign and does not change significantly for the last ~ 50 Myr for most models. This implies that a more robust comparison between the predicted present $\dot{\theta}_d$ and the observed one can be done.

The angular momentum vector (\mathbf{L}_d) is derived by using all disk particles within 21 kpc of the Galaxy in the present study. Accordingly it is possible that θ_d can be due largely to the outer warp formed in the disk during the LMC-Galaxy interaction. We investigate \mathbf{L}_d for $R = 3.5$ kpc, 8.5 kpc, and 21 kpc of the Galaxy at the final time step in the standard model and confirm that the angle between \mathbf{L}_d for $R = 8.5$ (3.5) kpc and 21 kpc is only 0.02° (0.001°). This means that if the Galaxy shows the pole shift, then the entire disk shows the pole shift (i.e., not simply due to the warp).

2.6 Parameter study

Although we have investigated a very large number of models, we describe the results of the 27 representative models in the present study. The orbital plane of the LMC is almost the same as that adopted in previous works by GN96 for all models. The Table 1 summarizes the model parameters for these representative models (T1 \sim T24) and for isolated models (I1 \sim I3). No LMC-Galaxy interaction is included in the three isolated models. Models in which the LMC experiences only one pericenter passage are referred to as "first passage" models, while those in which it experiences more are referred to as "multiple-passage" models.

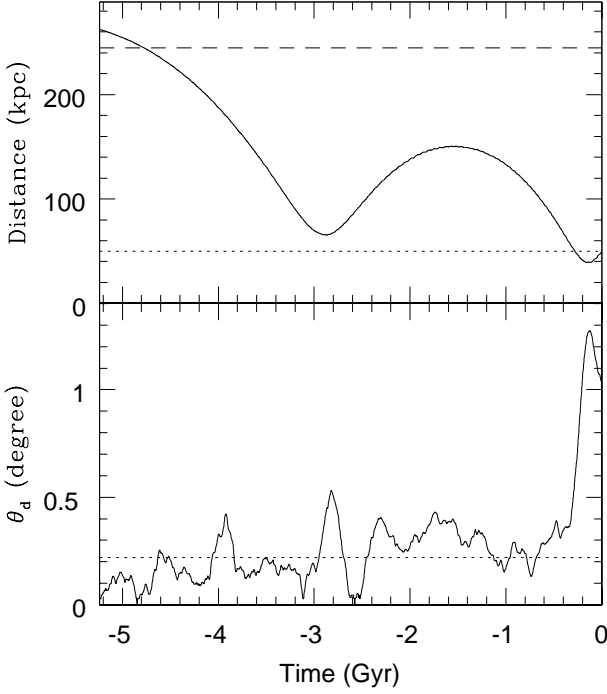


Figure 8. The time evolution of the distance between the LMC and the Galaxy (upper) and θ_d (lower) for the standard model (T1). The present LMC-Galaxy distance and the virial radius of the Galaxy are shown by dotted and dashed lines, respectively, in the upper panel. The maximum value of θ_d for ~ 2 Gyr isolated evolution of the Galaxy in the model I1 is shown by a dotted line in the lower panel for comparison.

We mainly describe the results of the “standard model” (T1), because we think that (i) the model parameters are quite reasonable and (ii) it shows more clearly the possible influences of the LMC on the evolution of the Galaxy. The LMC can not show $R = 50$ kpc within ~ 8 Gyr in some models with lower total masses of the LMC so that the result of these models are not useful in discussing the influences of the LMC on the Galaxy. However these models are quite useful in discussing the possible minimum LMC mass above which the LMC can have $R = 50$ kpc within a reasonable time scale. We thus discuss the results of these models in the Appendix A.

The EDC is much more significantly influenced by the LMC in comparison with the main stellar disk. We therefore mainly discuss the final structure and kinematics of the EDC in each model. We consider that the Galactic precession/nutation/pole-shift by distant tidal encounters between the Galaxy and its satellite galaxies are quite important in the Galactic astrometry. Therefore, we discuss the results of the models in which the parameter values are not reasonable for the LMC but possible for other satellite galaxies and previous infall of small groups in the Appendix B. Since we have already described the 3D distribution of stars stripped from the LMC stellar halo and discussed the importance of the distribution in understanding the past 3D orbit of the LMC in Bekki (2011), we only briefly discuss the distribution in the Appendix C.

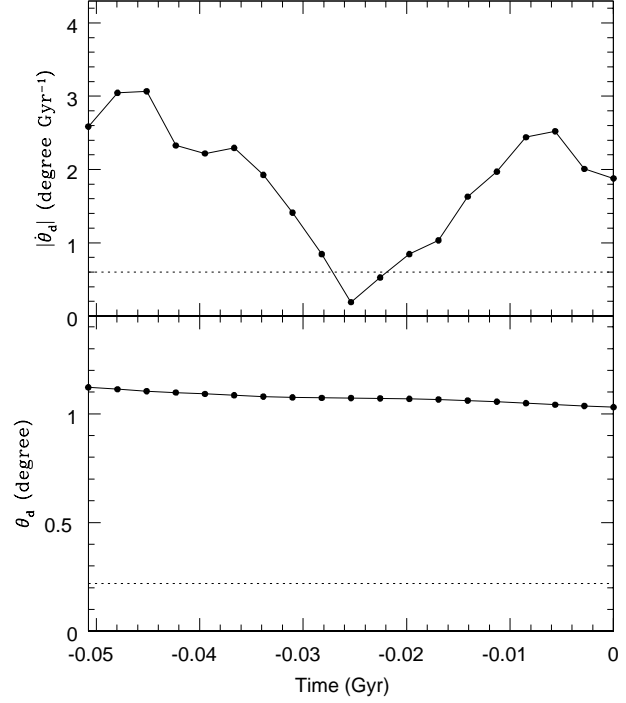


Figure 9. The time evolution of $\dot{\theta}_d$ (upper) and $|\theta_d|$ (lower) for the last ~ 0.05 Gyr in the standard model. The maximum values of $\dot{\theta}_d$ and θ_d for ~ 2 Gyr isolated evolution of the Galaxy in the model I1 are shown by dotted lines for comparison.

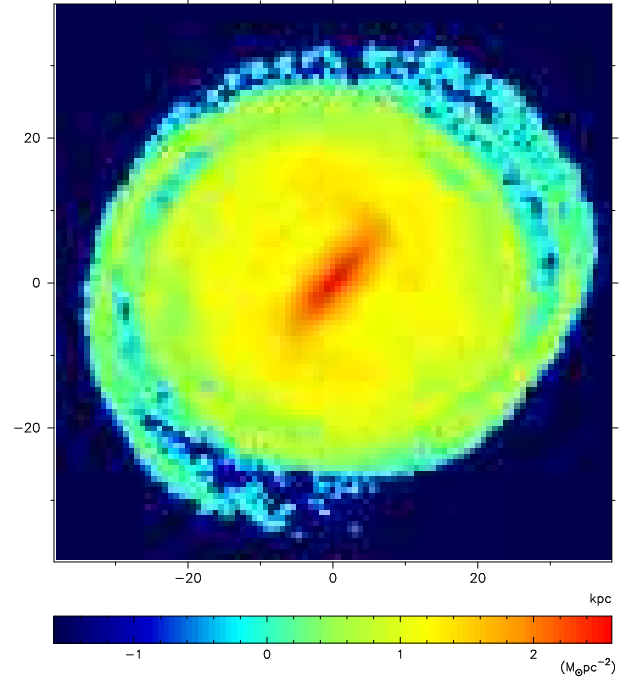


Figure 10. The same as Fig. 2 but for the present EDC (i.e., 0 Gyr) of the Galaxy in the standard model.

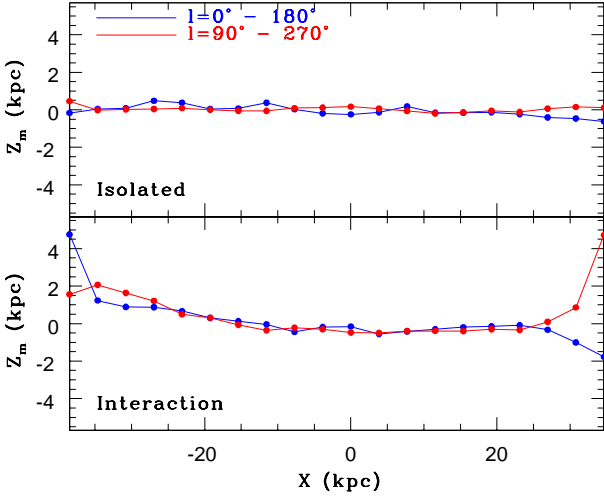


Figure 11. The mean z -position (Z_m) for the stars in the EDC of the Galaxy as a function of the projected distances (X) for the isolated model I1 (upper) and the standard interaction model T1 (lower). The blue and red lines show the Z_m profiles for the x - z projection (i.e., for $l = 0^\circ - 180^\circ$) and the y - z one (i.e., for $l = 90^\circ - 270^\circ$), respectively.

3 RESULTS

3.1 The standard model

Fig. 5 shows the orbital evolution of the LMC with respect to the Galactic center in the standard LMC-Galaxy interaction model T1. The radial scale length and vertical scale height of the EDC in this model are $0.4R_d$ (7 kpc) and $0.02R_d$ (0.35 kpc), respectively. The LMC passes its pericenter ($R = 65$ kpc) for the first time about 2.9 Gyr ago and for the second time about 0.2 Gyr ago in this model. The orbit of the LMC is almost an polar one and its orbital plane of the LMC is almost identical to the y - z plane. Fig. 6 shows that the distributions of the dark matter halo of the LMC at four representative time steps. After the first pericenter passage, the LMC can lose a significant fraction of its dark matter halo to the outer part of the Galaxy. About $\sim 33\%$ of the halo within $10R_{d,1}$ can be stripped by the strong tidal field of the Galaxy within the latest 5.2 Gyr. The stripped dark halo can form a ring-like distribution in the Galactic halo and could possibly influence the orbital evolution of other Galactic satellite galaxies.

Figs. 6 and 7 show how the first and the second LMC-Galaxy tidal encounters (i.e., the two pericenter passages) dynamically influences the EDC of the Galaxy. The first LMC-Galaxy encounter can only slightly influence the very outer part ($R > 30$ kpc) of the EDC: the outer EDC is slightly warped in the x - z plane. After the second LMC-Galaxy encounter, the present EDC of the Galaxy projected onto the x - z and y - z planes shows a clear sign of warps in its outer part ($R > 20$ kpc). The EDC projected onto the y - z plane appears to have a “bow-like” morphology (i.e., the two edges of the EDC are in the regions with $z > 0$). Given that the isolated disk model (I1) does not show such warp-like structures (later shown in Fig. 11), these results clearly demonstrates that the LMC-Galaxy tidal interaction can induce warps in the outer part of the EDC. This is confirmation of the results of previous simulations that show

the formation of the Galactic warps by the LMC-Galaxy interaction (e.g, Tsuchiya 2002; Weinberg & Blitz 2006).

As shown in Figs. 6 and 7, the disk stars of the LMC can not be stripped by the strong tidal field of the Galaxy, though the stellar disk can be dynamically heated up to form a thick disk. This no stripping of the LMC disk stars is due to the fact that the original LMC mass within $2R_{d,1}$ ($=15$ kpc) is $\sim 4 \times 10^{10} M_\odot$ for the LMC to have the maximum circular velocity of $\sim 110 \text{ km s}^{-1}$. If the original mass of the LMC is significantly smaller, then the stellar disk of the LMC can be stripped, as shown in the low-mass LMC model by BC05. The LMC can develop a strong stellar bar in the inner region of the disk during the LMC-Galaxy tidal interaction. The inner part of the LMC ($< 2R_{d,1} = 35$ kpc) can keep about 85% of its original mass after the 5.2 Gyr LMC-Galaxy tidal interaction.

Fig. 8 shows the time evolution of the LMC-Galaxy distance and θ_d . Clearly the inclination angle of the stellar disk in the Galaxy can suddenly increase and decrease before and after the first pericenter passage about ~ 3 Gyr ago. Although the change of θ_d is small (i.e., less than one degree), this sudden change may well be better described as “pole shift” rather than regular precession/nutation. After the first pericenter passage, the stellar disk of the Galaxy can continue to keep a higher θ_d till 0.4 Gyr ago. The disk can increase significantly and suddenly θ_d during second pericenter passage owing to the gravitational torque of the LMC. The disk decrease θ_d after the second pericenter passage and finally it has $\theta_d = 1.0^\circ$ and $\phi_d = 125.5^\circ$ (at the present).

Fig. 9 shows the time evolution of θ_d and the change rate ($\dot{\theta}_d$) for the last ~ 0.05 Gyr. The value of θ_d at the final time step can correspond to the present pole-shift rate of the Galaxy. Here we use the term “pole-shift rate” just for convenience and clarity, though the long-term precession/nutation is not a regular one. Clearly, θ_d decreases quite steadily for the last 0.05 Gyr, though the time evolution of $\dot{\theta}_d$ is slightly irregular. The negative values of $\dot{\theta}_d$ for the last 0.05 Gyr strongly suggest that the Galactic disk will continue to decrease θ_d in the future (at least till the LMC passes its third pericenter). The present pole-shift rate is estimated as $1.9 \text{ degree Gyr}^{-1}$ corresponding to $\sim 6.8 \mu\text{as yr}^{-1}$ in this standard model. The derived $\dot{\theta}_d$ in the standard model is significantly larger than that (at most $0.6 \text{ degree Gyr}^{-1}$) derived for the isolated model I1. Therefore the higher pole-shift rate can be regarded as being due to the LMC-Galaxy interaction.

Fig. 10 shows that the distribution of the EDC projected onto the x - y plane (i.e., the Galactic plane) appears to be significantly elongated and significantly distorted. Furthermore, the outer part of the EDC has two distinct spiral-arm structures, which were formed as a result of the last LMC-Galaxy tidal interaction. These spiral-arm structures might well correspond to the distant ($18 \text{ kpc} < R < 24 \text{ kpc}$) extended spiral arms of the Galaxy discovered by McClure-Griffiths et al. (2004). The central bar in the EDC is formed not from the LMC-Galaxy interaction but from the dynamical interaction between the newly developed stellar bar of the Galaxy and the EDC. These results strongly suggest that the outer part ($R > 20$ kpc) of the Galactic gas disk can have a significantly asymmetric distribution owing to the LMC-Galaxy tidal interaction. Thus both the vertical structure of the Galaxy (e.g., the presence of the warps)

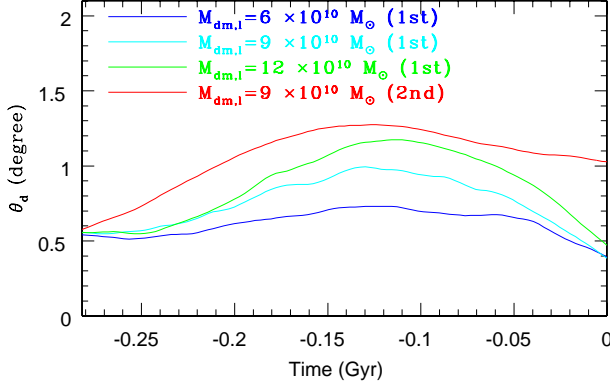


Figure 12. The time evolution of θ_d for the last 0.28 Gyr in the four different models: T19 with $M_{\text{dm},l} = 6 \times 10^{10} M_\odot$ and $f_v = 1.12$ (blue), T18 with $M_{\text{dm},l} = 9 \times 10^{10} M_\odot$ and $f_v = 1.12$ (cyan), T20 with $M_{\text{dm},l} = 12 \times 10^{10} M_\odot$ and $f_v = 1.12$ (green), and T1 with $M_{\text{dm},l} = 9 \times 10^{10} M_\odot$ and $f_v = 0.63$ (red). The first three models are first passage models with higher present velocities of the LMC. The model with $f_v = 0.63$ is the standard model.

and the non-asymmetric structure of the outer Galaxy have fossil information of the past LMC-Galaxy interaction history.

Fig. 11 shows the mean z -position (Z_m) of the stars in the EDC as a function of the projected positions (X). In the Galactic coordinate system adopted in the present study, the location of the Sun is set to be $(-8.5, 0, 0)$ kpc. Therefore the positive (negative) direction of the x -axis points to $l = 0^\circ$ ($l = 180^\circ$) whereas the positive (negative) direction of the y -axis points to $l = 90^\circ$ ($l = 270^\circ$). The Z_m profile for the stars in the EDC projected onto the x -axis clearly shows a warp with the morphology similar to an “integral symbol”: the warp structure has a positive Z_m for $x < -20$ kpc and a negative Z_m for $x > 20$ kpc. The Z_m profile for the stars projected onto the y -axis also shows a warp with a “bow-like” shape (i.e., positive Z_m both for $y < -20$ kpc and for $y > 20$ kpc). These results demonstrate that the shape of the Galactic bar can depend on from where it is observed.

The LMC-Galaxy interaction can also influence the kinematics of the EDC in the Galaxy. The present vertical velocity dispersion (σ_z) of the EDC at $R = 26$ kpc in the isolated model is 4.0 km s^{-1} whereas it is 5.7 km s^{-1} in the standard model (i.e., with LMC-Galaxy interaction). The difference in σ_z between the two models can be also clearly seen for $R > 20$ kpc. For example, σ_z at $R = 35$ kpc in the isolated model is 2.8 km s^{-1} whereas it is 3.4 km s^{-1} in the standard model. These results clearly demonstrate that the outer kinematics of the extended stellar and gaseous disks of the Galaxy have fossil information on the past LMC-Galaxy tidal interaction.

3.2 Parameter dependences

3.2.1 Galactic precession

(1) The time evolution of θ_d and $\dot{\theta}_d$ depends on $M_{\text{dm},l}$, $f_{v,t}$ and $f_{v,r}$, because the orbital period and the last pericenter distance of the LMC (R_p) strongly depend on the three parameters. The present θ_d is likely to be larger for models with larger $M_{\text{dm},l}$ for a given set of orbital parameters ($f_{v,t}$

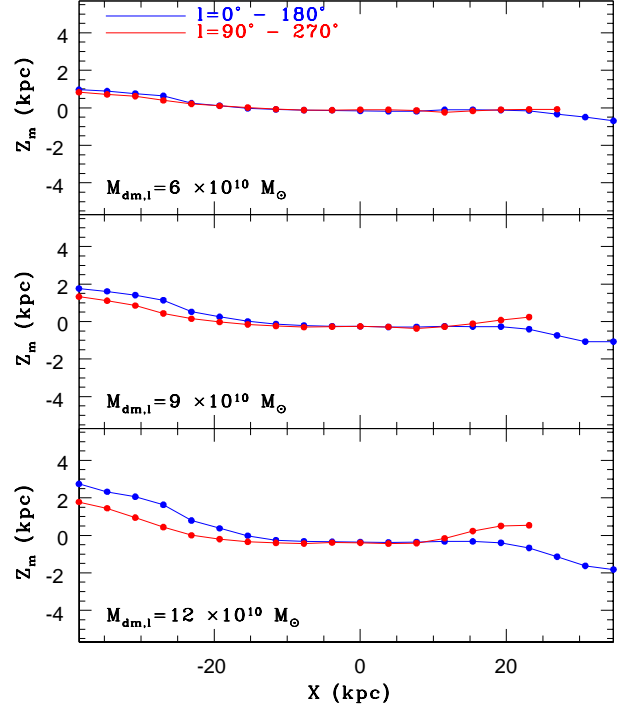


Figure 13. The same as Fig. 11 but for three different first passage models with $M_{\text{dm},l} = 6 \times 10^{10} M_\odot$ (top), $M_{\text{dm},l} = 9 \times 10^{10} M_\odot$ (middle), and $M_{\text{dm},l} = 12 \times 10^{10} M_\odot$ (bottom). Here Z_m is shown for radial bins with particles (if no particle is found in a bin, Z_m is not plotted for the bin).

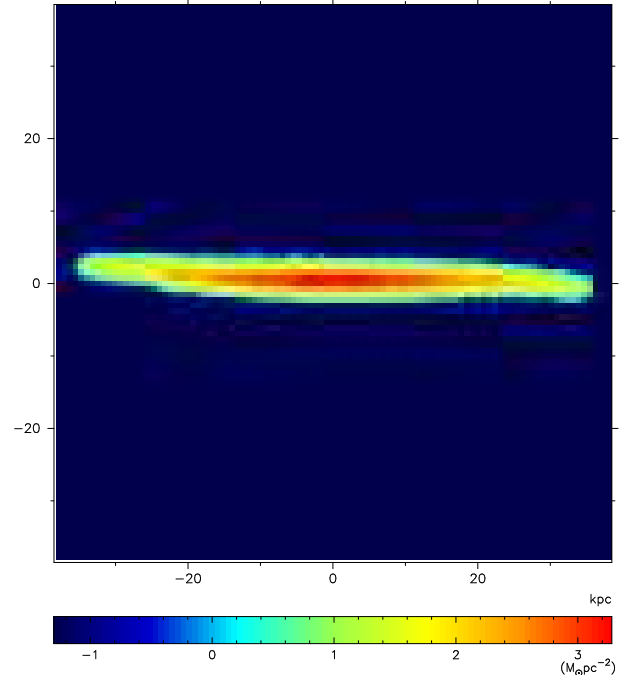


Figure 14. The same as Fig. 10 but for the x - z projection in the model T18. Owing to the short-term evolution (~ 1.4 Gyr), a bulge-like component in the EDC can not form in this model.

and $f_{v,r}$), because the tidal perturbation from the LMC is stronger thus can more strongly influence the dynamical evolution of the Galaxy. Both multiple passage and first passage models show *negative* $\dot{\theta}_d$ in the present Galaxy. The Galaxy shows the maximum θ_d at the pericenter passage of the LMC and then θ_d decreases. Therefore, the present Galaxy, which is just after the pericenter passage of the LMC, can show *negative* $\dot{\theta}_d$.

(2) Although the present θ_d is smaller in first passage models than in multiple ones, $\dot{\theta}_d$ is larger in first passage models. Fig. 12 shows the time evolution of θ_d for the three first passage models with different $M_{dm,l}$ yet the same $f_{v,t}$ and $f_{v,r}$. The present θ_d and the present absolute magnitude of θ_d are larger for models with larger $M_{dm,l}$ in the three models.

(3) The mean θ_d and $|\dot{\theta}_d|$ for these models are 0.64° and $4.6 \text{ degree Gyr}^{-1}$, respectively. These results strongly suggest that the Galactic precession/nutation/pole-shift due to the last LMC-Galaxy tidal encounter can be detected by future observational studies by GAIA, if there is a novel method to detect the Galactic precession/nutation/pole-shift. We discuss future observational studies by GAIA for the detection of the Galactic precession/nutation/pole-shift later in §4.

3.2.2 The influences on the EDC

(1) The present outer structure of the EDC in the Galaxy depends more strongly on $M_{dm,l}$ rather than on $f_{v,t}$ and $f_{v,r}$ both in first passage and multiple passage models. Fig. 13 shows that the warps of the EDCs can be more clearly seen in first passage models with larger $M_{dm,l}$ owing to stronger tidal perturbation of the LMC. Although the models with $M_{dm,l} = 9 \times 10^{10} M_\odot$ and with $M_{dm,l} = 1.2 \times 10^{11} M_\odot$ show warp-like structures in the outer regions of the EDCs, the models with $M_{dm,l}$ less than $6 \times 10^{10} M_\odot$ do not clearly show such structures. Fig. 14 shows that the EDC in the first passage model with $M_{dm,l} = 9.0 \times 10^{11} M_\odot$ (T18) has a warp-like structure, in particular, in the outer regions with negative x .

(2) The outer region of the EDC in the model with lower M_{dm} (T19 with a lower mass of the Galactic dark matter halo) can be too severely damaged by the LMC-Galaxy tidal interaction. This result implies that if the LMC has an original mass of $\sim 10^{11} M_\odot$, the Galaxy should already have enough a large mass ($\sim 10^{12} M_\odot$) about several Gyr ago to avoid too much damage of its outer part due to the LMC-Galaxy interaction. Equally, if the Galaxy has a significantly smaller mass when the LMC enters into the Galaxy for the first time, then the initial mass of the LMC should be small enough to suppress the destruction of the EDC of the Galaxy.

(3) The present structures of the EDCs depend also on the initial size (R_{edc}) such that the dynamical influences of the past LMC-Galaxy interaction can be less clearly seen in the models with smaller R_{eds} . For example, warp-like structures can not be so clearly seen in the model T16 in comparison with the model T17 (and T1). Whether the simulated warps look like an “integral symbol” or a “bow” depends on the viewing angles of observers.

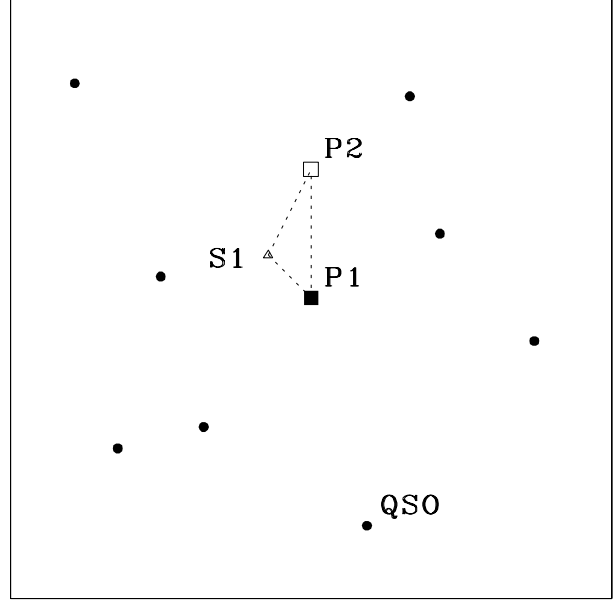


Figure 15. An illustrative figure for describing the proposed new method by which we can possibly detect the Galactic precession. The QSOs (or extragalactic radio sources) are shown by filled circles, and the locations of a hypothetical “fixed point” (e.g., the Sgr A*) in the two observations done at two different epochs are denoted as P1 and P2. The fixed point (e.g., Sgr A*) moves from P1 to P2 owing to (i) the Galactic precession (from P1 to S1) and (ii) the solar motion with respect to the Galactic center (from S1 to P2).

4 DISCUSSION

4.1 The Galactic precession

The present study has first demonstrated that the LMC-Galaxy interaction can induce the irregular precession/nutation/pole-shift of the Galaxy. From now on in this section, we simply use the term “precession” to describes the irregular precession/nutation or pole shift just for convenience. The mean value of the simulated present precession rates ($\dot{\theta}_d$) is about $4.6 \text{ degree Gyr}^{-1}$ corresponding to $16.6 \mu\text{as yr}^{-1}$. The derived $\dot{\theta}_d$ can be detected by future astrometry satellites with μas precision like GAIA, though there should be a novel way to investigate the rate and the direction of the Galactic precession. The LMC-Galaxy interaction would not be a sole mechanism for the induction of the Galactic precession: minor merging (e.g., Quinn & Goodman 1986) and gas accretion onto the Galactic disk would also cause the Galactic precession. The predicted precession direction and rate would be different between different mechanisms, future observations would be able to give strong constraints on which mechanism would be the most reasonable for the possible precession. Below we briefly discuss the implications of the ongoing Galactic precession and a possible way to detect the precession.

4.1.1 Implications

If the Galactic precession is really ongoing, then it has a number of important implications. First, changes in the x -, y -, and z -positions of an astronomical object (outside the

Galactic disk) in the Galactic coordinate system for a certain period of time can be due to the combination of (i) the real change of the 3D position with respect to the Galactic center and (ii) the slight change in the orientation of the rotating axis of the Galactic disk. However, the latter effect (ii) would be significantly smaller (e.g., $\dot{\theta}_d \approx 4.6 \times 10^{-9}$ degrees yr^{-1} or $16.6 \mu\text{as yr}^{-1}$ for the possible LMC infall) in comparison with the former (i) for most astronomical objects close to the Galaxy. Second, the inclination angles of orbital planes of the outer Galactic satellite galaxies with respect to the Galactic plane can be different between past and present because of the recent tilting of the disk (not because of their orbital changes due to dynamical friction etc), if the satellite galaxies were accreted onto the Galaxy well before previous group infall.

Third, reconstruction of the past orbit of a Galactic satellite galaxy using N-body simulations should be done more carefully. Almost all previous models to reproduce the observed stellar and gaseous streams formed from tidal destruction of Galactic satellite galaxies (e.g., the Sgr dwarf and the SMC) assumed a *fixed* Galactic potential (e.g., GN96; Law & Majewsky 2010). However, if the Galactic precession has been ongoing until recently, as suggested by the present study, then the adopted assumption of the fixed Galactic potential can be no longer valid: the time-dependent disk potential due to the tilting disk would need to be considered, in particular, for those orbiting close to the disk.

4.1.2 How can we detect ?

If the Galactic precession is real, then locations of distant QSOs and extragalactic radio sources can not be used as (background) fixed points *in the Galactic coordinate* to measure the proper motions of the Galactic stars in a very precise way: the locations of distant QSOs in the Galactic coordinate system can change due to the precession. Owing to the location of the Sun with respect to the Galactic center and its move within the Galaxy, the changes in the locations of QSOs in the Galactic coordinate are due to (i) the Galactic precession and (ii) the change of the Sun's location with respect to the Galactic center: the Galactic coordinate system depends on the location of the Sun (see Fig. 15 for an illustrative purpose). Here we consider that it is reasonable to refrain from using the Galactic coordinate system and instead to use distant QSOs as fixed points on the sky.

We thus propose the following method to detect a possible Galactic precession by using the background QSOs. In this method, the QSOs are assumed to be fixed points on the sky and the location of the exact center of the Galaxy (the radio source Sagittarius A*, Sgr A*, denoted as “P1” and “P2” in Fig. 15) is investigated at different two observations done at two different epochs with a certain time interval (e.g., two years). The position of Sgr A* on the sky in each of the two observations is estimated with respect to nearby QSOs. The positional change of Sgr A* (from P1 to P2) between the two observations is due to (i) the Galactic precession (from P1 to S1) and (ii) the solar motion (from S1 to P2). Therefore, if we can separately estimate the contribution from the solar motion (i.e., a vector connecting between S1 and P2), then we can have some information on

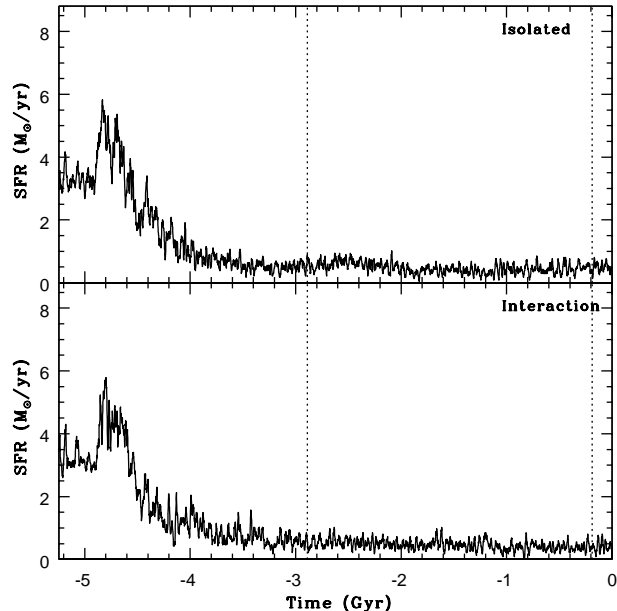


Figure 16. The time evolution of star formation rates in the isolated model (upper) and the interaction one (lower). The epochs of the two pericenter passages of the LMC are shown by dotted lines.

the Galactic precession (i.e., a vector connecting between P1 and S1).

The potential problem of the above method is that it would be difficult to derive the contribution of the Sun's motion: we need to predict very precisely how the Sun moves with respect to Sgr A* to detect observationally the Galactic precession. Recently Reid & Brunthaler (2004) have investigated the proper motion of Sgr A* with respect to two extragalactic radio sources using VLBI and found that the apparent proper motion of Sgr A* relative to J1745-283 is 6.379 ± 0.024 mas yr^{-1} . They claimed that (i) the proper motion can be largely explained by the orbit of the Sun around the Galaxy and (ii) the residual proper motion perpendicular to the plane of the Galaxy is -0.4 ± 0.9 km s^{-1} . This residual could have some information on the Galactic precession, though there could be some observational uncertainties in the solar motion within the Galaxy.

Although Sgr A* is considered to be a hypothetical fixed point in the above method, other fixed points (if any) within the Galaxy can be proposed. There could be other possible methods to detect the Galactic precession, but we currently do not have any better ones. Although Hipparchus discovered the evidence of the Earth's precession more than 2000 years ago, the possibility of the *ongoing* Galactic precession (and pole shift) and the likely impact of the precession in the modern astronomy have not been extensively discussed by observational and theoretical studies so far. Given the μas accuracy of future astrometry satellites, now the time seems to be ripe for extensive discussion on the origin of the possible Galactic precession and pole shift.

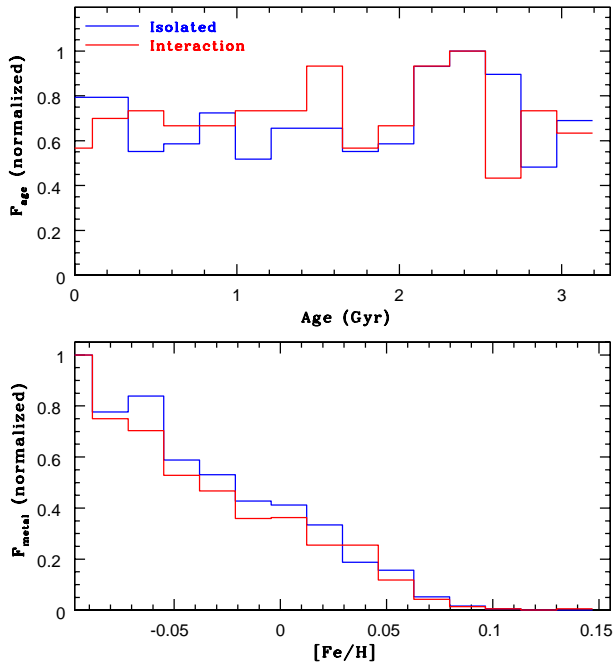


Figure 17. The age (upper) and metallicity (lower) distributions of new stars formed from gas in the Galaxy for the isolated (blue) and interaction (red) models. The distributions are normalized by the maximum number of stars in the 20 age and metallicity bins.

4.2 The Galactic star formation history influenced by the LMC ?

Rocha-Pinto et al. (2000) investigated the age distribution of 552 late-type dwarfs and thereby derived the star formation history of the Galaxy. They showed that the disk of the Galaxy has experienced enhanced episodes of star formation at 0–1 Gyr, 2–5 Gyr, and 7–9 Gyr ago and suggested that these enhanced episodes can be closely associated with the interaction between the Magellanic Clouds and the Galaxy. There could be a number of physical mechanisms responsible for the observed possible enhancement of the Galactic star formation: for example, minor merging and rapid infall of high velocity clouds could enhance significantly star formation in some local regions of the Galaxy. However, we here focus exclusively on whether the LMC-Galaxy tidal interaction can significantly change the star formation history of the Galaxy.

In order to discuss the possible influence of the LMC-Galaxy interaction on the Galactic star formation history, we use chemodynamical numerical simulations with star formation and chemical evolution. Since our GRAPE-based and GPU-based numerical codes are only for collisionless system, we adopt our TREESPH code used in our previous numerical simulations on the formation of stars and globular clusters in interacting galaxies (see Bekki et al. 2002 for definitions and details). We do not include the model for globular cluster formation (that was modeled in Bekki et al. 2002) in the present investigation. We adopt the present low-resolution model and add a gas disk with an exponential radial profile to the Galaxy so that star formation from gas can be investigated. The gas disk has a size of $2R_d$, a scale length of $0.4R_d$, and a scale height of $0.02R_d$, and a mass of $0.2M_d$. Initially the gas disk has a metallicity of 0.016 and

the chemical yield and the return parameter in the chemodynamical model are set to be 0.01 and 0.3, respectively. An isothermal equation of state is adopted for the gas with a temperature of 10^4 K.

Fig. 16 shows the star formation history of the Galaxy in the model in which the model parameters are the same as those used in the standard model. For comparison, the star formation history in the isolated model (i.e., without interaction with the LMC) is shown. Clearly, there is no dramatic difference in the star formation history of the Galaxy between the two models, which suggests that the LMC can not change significantly the *global star formation history* of the Galaxy (e.g., the mean star formation rate for the last several Gyr) through its tidal interaction with the Galaxy. The star formation rate of the Galaxy can not be enhanced by the last LMC-Galaxy interaction about 0.2 Gyr ago, though the LMC can strongly influence the outer part of the Galactic disk. There appears to be a small difference in the Galactic star formation history ~ 1 Gyr after (i.e., ~ 1.6 Gyr ago) the first pericenter passage of the LMC between the two models: the LMC’s tidal force could possibly have a very minor influence on the Galactic star formation. But the difference is as small as the noise fluctuation, and thus we can not claim that the LMC can increase global star formation rate of the Galaxy in the present study.

Fig. 17 shows the present age and metallicity distributions of new stars formed from gas for the disk region with $7.0 \text{ kpc} \leq R \leq 10 \text{ kpc}$ (i.e., the solar-neighborhood) in the isolated and interaction models. Although the differences in the age distribution between the isolated and interaction models can be barely seen (the difference can be as small as the noise fluctuation), there is no outstandingly clear peak at an age of ~ 3 Gyr when the first LMC-Galaxy encounter can possibly influence the star formation history in the solar-neighborhood. Furthermore there is no clear peak in the age distribution of the interaction model at an age of 0.1 – 0.2 Gyr where the last LMC-Galaxy tidal encounter occurs. These results imply that it is a formidable task for observational studies to find the possible evidence (e.g., a burst epoch of star formation) for the Galactic star formation in the solar-neighborhood influenced by the LMC-Galaxy interaction. As shown in Fig. 17, there are some differences in the metallicity distributions of stars in the solar-neighborhood between the isolated and interaction models. Although the differences enable us to claim that the LMC-Galaxy interaction can slightly change the metallicity distribution of the stars, they do not provide strong constraints on when the LMC-Galaxy interaction strongly influenced the star formation in the solar-neighborhood.

4.3 The distribution of the stripped satellite galaxies from the LMC group

So far we have described the results of the models in which dwarfs are not included, though the LMC could have been accreted onto the Galaxy as a group with a number of dwarfs (e.g., Bekki 2008). The reason for this non-inclusion is that small galaxy groups are dominated by massive dark matter halos (i.e., the total masses of group member dwarfs are quite small) so that the orbital evolution of the groups can be determined largely by the total masses of dark matter initially in the groups. Indeed, even if 20 dwarfs with the

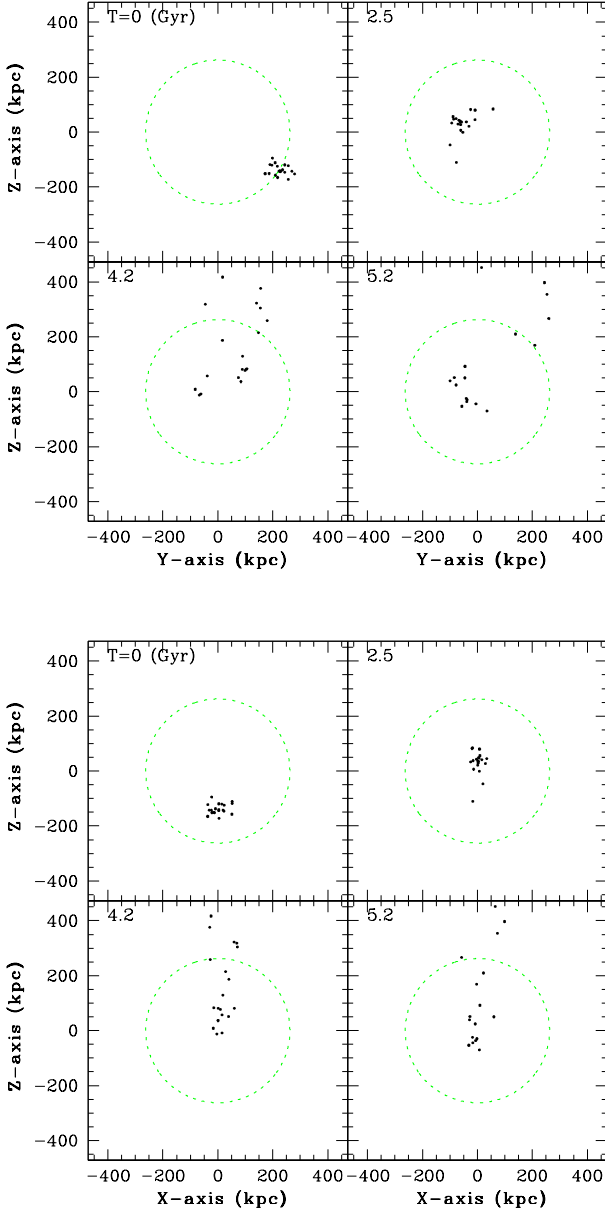


Figure 18. The time evolution of the distribution of the 20 dwarfs initially in the LMC group projected onto the y - z plane (upper four) and the x - y one (lower). The virial radius of the Galaxy is shown by a green dashed line in each panel.

total mass being 0.1% of the total mass of the dark matter in a group are added to the group, the present results do not change at all. The models with 20 equal-mass dwarfs (i.e., the models T23 and 24) are useful in discussing how the infall of the LMC with dwarfs can change the distribution of the Galactic satellite galaxies.

One of interesting results in the model T23 with 20 dwarfs is that the group member dwarfs show a thin disk-like distribution along the z -axis within $R < 400$ kpc in the Galaxy. As shown in Figure 11, the thin distribution of the group member dwarfs (some of which are tidally stripped during group infall) is closely associated with the dark disk formed during group infall. This result implies that the observed thin disk of the Galactic satellite galaxies along the

Galactic polar axis (e.g., Metz et al. 2009) can be understood in the context of a previous group infall event of the LMC around the Galaxy. The final distribution of the dwarfs stripped from the LMC depends on R_{dw} such that the thin distribution of the stripped dwarfs can be more clearly seen in the model with larger R_{dw} (T23 compared to T24). Recently Nichols et al. (2011) have shown that Draco, Sculptor, Sextans, Ursa Minor, and the Sagittarius Stream are consistent with them initially in the LMC group, though their models are rather idealized (using test particle simulations).

It should be noted here that two dwarfs can sink into the inner region of the LMC disk ($R < R_{\text{d},1}$) owing to dynamical friction against the halo in the model T24 with $R_{\text{dw}} = 5R_{\text{d},1}$: these dwarfs can be regarded as being merged with the LMC. This possible merging between the LMC and the group member dwarfs does not occur in the model T23 with $R_{\text{dw}} = 10R_{\text{d},1}$. Although a possible minor merger event in the LMC was discussed in the context of the observed possible counter-rotating component of stars in the LMC (e.g., Subramaniam & Prabhu 2005), its influence on the LMC's evolution (e.g., the thick disk formation) has not been discussed extensively in previous theoretical studies. It is thus our future study how such a minor merger event can change the star formation history and dynamical evolution of the LMC.

5 CONCLUSIONS

We have developed a new method by which we can reproduce rather precisely and efficiently the present location of the LMC in self-consistent N-body numerical simulations of orbital evolution of the LMC in a live gravitational potential of the Galaxy. Using this new method (called “CTM”), we have investigated the orbital evolution of the LMC from outside the virial radius of the Galaxy and its influence on the evolution of the Galaxy in a self-consistent manner for a given set of model parameters of the LMC and the Galaxy. The principle results are summarized as follows.

(1) The LMC-Galaxy tidal interaction can cause the “pole shift” (or irregular precession/nutation) of the Galaxy with the present pole-shift rate $\dot{\theta}_{\text{d}}$ being ~ 2 degree Gyr^{-1} (corresponding to $\sim 7\mu\text{as yr}^{-1}$), if the original mass of the LMC before its entrance into the virial radius of the Galaxy is as large as $9 \times 10^{10} M_{\odot}$. The values of the present $\dot{\theta}_{\text{d}}$ depend on $M_{\text{dm},1}$ and orbits of the LMC, and the mean $\dot{\theta}_{\text{d}}$ for models that reproduce the present location of the LMC is ~ 4.6 degree Gyr^{-1} (corresponding to $16.6 \mu\text{as yr}^{-1}$).

(2) The outer part ($R > 20$ kpc) of the extended disk component (EDC) of the Galaxy can be influenced by the LMC-Galaxy tidal interaction, in particular, when the LMC passes through its last pericenter of the orbit. As a result of this, the outer part of the EDC shows warp-like structures in most models. The detailed morphologies of the warps (e.g., “integral symbol” or “bow-like”) depend on the viewing angles of observations and $M_{\text{dm},1}$. The present study thus confirms the results of previous theoretical studies on the formation of the Galactic warp by the LMC-Galaxy interaction.

(3) The LMC-Galaxy tidal interaction can also be responsible for the formation of elongated and asymmetric (e.g., spiral-like) structures in the outer part of the EDC.

The interaction can dynamically heat up the EDCs so that the vertical velocity dispersions of the outer parts ($R > 20$ kpc) of the EDCs in the tidal models can be significantly larger than those in the isolated models. The structure and kinematics of the EDC depend on the original mass and the orbit of the LMC. The outer part of the Galaxy can thus have fossil records of the past LMC-Galaxy tidal interaction. The LMC-Galaxy interaction can change the outer structure and kinematics of the Galaxy also in first passage models.

(4) The global star formation history of the Galaxy for the last several Gyr (e.g., the mean star formation rate across the Galaxy) can not be significantly influenced by the LMC-Galaxy dynamical interaction, if the initial $M_{\text{dm},i}$ is less than $1.2 \times 10^{11} M_{\odot}$. The star formation history and the age-metallicity relation of stars at the solar-neighborhood ($7 < R < 10$ kpc defined in the present study) can be only slightly influenced by the LMC-Galaxy interaction. However, these results need to be re-investigated and confirmed by future more sophisticated and higher resolution numerical simulations.

(5) If the LMC is accreted onto the Galaxy as group with dwarfs, then the stripped dwarfs during the group infall can show a thin disk-like distribution along the z -axis within $R < 400$ kpc around the Galaxy. The distribution of the dwarfs follows the disk/ring-like distribution of dark matter stripped from the group. Therefore, both the possible Galaxy precession/nutation/pole-shift and the observed thin distribution of the Galactic satellite galaxies can share a common origin (i.e., the infall of the LMC group). A few of the dwarfs in the group can merge with the LMC during the infall of the LMC, if the initial distribution of the dwarf is more compact.

(6) The derived $\dot{\theta}_d$ of the Galaxy caused by the LMC infall is suggested to be able to be detected by future astrometric satellites with μas precision (such as GAIA). The possible Galactic precession has a number of important implications in galactic astronomy, such as the observational derivation of the proper motions of Galactic satellite galaxies using the background QSOs. A possible way to detect the ongoing precession of the Galaxy has been briefly discussed.

(7) We conclude that the dynamical evolution of the outer part (> 20 kpc) of the Galaxy can be influenced by the past long-term LMC-Galaxy tidal interaction. Therefore the structure and kinematics of the outer part of the Galaxy can have fossil records on when and how the LMC arrived in the Galaxy. It is doubtlessly worthwhile for future observational studies to investigate whether there is an imprint of the past LMC-Galaxy interaction in the star formation history of the solar-neighborhood.

6 ACKNOWLEDGMENT

I am grateful to the anonymous referee for constructive and useful comments that improved this paper. KB acknowledge the financial support of the Australian Research Council throughout the course of this work. The work was supported by iVEC through the use of advanced computing resources located at the University of Western Australia.

REFERENCES

- Bekki, K., 2008, *ApJ*, 684, L87
 Bekki, K., 2011, *MNRAS*, 416, 2359
 Bekki, K., Forbes, D. A., Beasley, M. A., Couch, W. J., 2002, *MNRAS*, 335, 1176
 Bekki, K., Chiba, M., 2005, *MNRAS*, 356, 680
 Besla, G., Kallivayalil, N., Hernquist, L., Robertson, B., Cox, T. J., van der Marel, R. P., Alcock, C., 2007, *ApJ*, 668, 949
 Connors, T. W., Kawata, D., & Gibson, B. K., 2006, *MNRAS*, 371, 108
 Costa, E., et al., 2009, *AJ*, 137, 4339
 Diaz, J., Bekki, K., 2011, *MNRAS*, 413, 2015 (DB11a)
 Diaz, J., Bekki, K., 2011, *PASA*, 28, 117 (DB11b)
 Diaz, J., Bekki, K., 2011, submitted to *ApJ*, in preprint (arXiv:1112.6191) (D11c)
 Gardiner, L. T., Sawa, T., Fujimoto, M., 1994, *MNRAS*, 266, 567
 Gardiner, L. T. & Noguchi, M., 1996, *MNRAS*, 278, 191 (GN96)
 Hunter, C., Toomre, A., 1969, *ApJ*, 155, 747
 Kallivayalil, N., van der Marel, R. P., Alcock, C., Axelrod, T., Cook, K. H., Drake, A. J., Geha, M., 2006, *ApJ*, 638, 772
 Keller, S. C., et al., 2007, *PASA*, 24, 1
 Law, D. R., & Majewski, S. R. 2010, *ApJ*, 714, 1128
 Levine, E. S., Blitz, L., Heiles, C., 2006, *ApJ*, 643, 881
 Li, Y., Helmi, A., 2008, *MNRAS*, 385, 1365
 Lin, D. N. C., Lynden-Bell, D., 1977, *MNRAS*, 181, 59
 Mastropietro, C., Burkert, A., Moore, B., 2009, *MNRAS*, 399, 2004 (M05)
 McClure-Griffiths, N. M.; Dickey, John M.; Gaensler, B. M.; Green, A. J., 2004, *ApJ*, 611, L145
 Metz, M., Kroupa, P., Theis, C., Hensler, G., Jerjen, H., 2009, *ApJ*, 697, 269
 Momany, Y., Zaggia, S., Gilmore, G., Piotto, G., Carraro, G., Bedin, L. R., de Angeli, F., 2006, *A&A*, 451, 515
 Murai, T., Fujimoto, M., 1980, *PASJ*, 32, 581
 Navarro, J. F., Frenk, C. S., White, S. D. M., 1996, *ApJ*, 462, 563 (NFW)
 Nichols, M., Colless, J., Colless, M. Bland-Hawthorn, J., 2011, in preprint
 Olsen, K. A. G., Massey, P., 2007, *ApJ*, 656, 61
 Piatek, S., Pryor, C., Olszewski, E. W., 2008, *AJ*, 135, 1024
 Quinn, P. J., & Goodman, J. 1986, *ApJ*, 309, 472
 Reid, M. J., Brunthaler, A., 2004, *ApJ*, 616, 872
 Rocha-Pinto, H. J., Scalo, J., Maciel, W. J., Flynn, C., 2000, *A&A*, 358, 869
 Ruzicka, A., Theis, C., Palous, J., 2010, *ApJ*, 725, 369
 Subramaniam, A., & Prabhu, T. P., 2005, *ApJL*, 625, 47
 Sugimoto, D., Chikada, Y., Makino, J., Ito, T., Ebisuzaki, T., Umemura, M., 1990, *Nat*, 345, 33
 Tsuchiya, T. 2002, *NewA*, 7, 293
 Vieira, K., et al. 2010, *AJ*, 140, 1934
 Weinberg, M. D., 1998, *MNRAS*, 299, 499
 Wilkinson, M. I., Evans, N. W., 1999, *MNRAS*, 310, 645
 Yoshizawa, A., Noguchi, M., 2003, *MNRAS*, 339, 1135 (YN03)

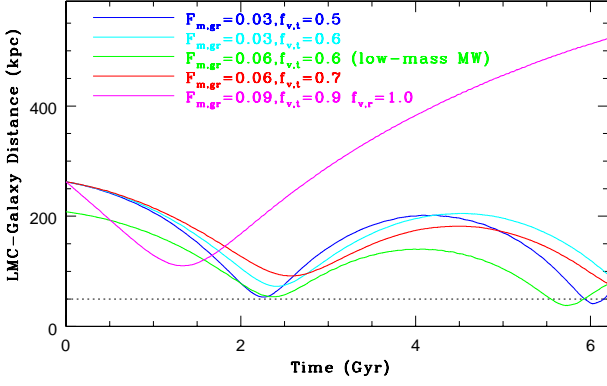


Figure A1. The orbital evolution of the LMC in the five models: $F_{m,gr} = 0.03$ and $f_{v,t} = 0.5$ (blue), $F_{m,gr} = 0.03$ and $f_{v,t} = 0.6$ (cyan), $F_{m,gr} = 0.06$ and $f_{v,t} = 0.6$ (green), $F_{m,gr} = 0.06$ and $f_{v,t} = 0.7$ (red), and $F_{m,gr} = 0.09$, $f_{v,t} = 0.9$, and $f_{v,r} = 1.0$ (magenta). For the models with $F_{m,gr} = 0.03$ and 0.06 , $f_{v,r} = 0.2$. The dark matter mass of the Galaxy in the model shown by a green line ($F_{m,gr} = 0.06$ and $f_{v,t} = 0.6$) is $5 \times 10^{11} M_{\odot}$ (i.e., the half of $M_{dm,mw}$ in other models). The present LMC-Galaxy distance is shown by a dotted line.

APPENDIX A: THE ORBITAL EVOLUTION OF THE LMC IN UNSUCCESSFUL MODELS

In the main text, we have mainly described the results on the “successful models” in which the observed position of the LMC can be reproduced well. The pericenter radius (R_p) of the LMC’s orbit around the Galaxy can not be as small as $R = 50$ kpc within ~ 8 Gyr in the “unsuccessful models” with lower $M_{dm,l}$ and higher f_v . This is because the time scale of dynamical friction of the LMC can be long (longer than the Hubble time) owing to the smaller LMC masses and the larger amount of initial orbital angular momentum in these models. Although these models are not useful in discussing the dynamical influences of the LMC on the Galaxy, they are quite useful in determining a range of f_v ($f_{v,t}$ and $f_{v,r}$) for realistic orbital models of the LMC and thus discussing how the LMC was accreted onto the Galaxy. Fig. A1 summarizes the results of five different models, three of which are regarded as unsuccessful models in the present study. The mass-ratio of $M_{dm,l}$ to $M_{dm,mw}$ is referred to as $F_{m,gr}$ for convenience and used in this and following appendix sections.

As shown in Fig. A1, the LMC can not have $R_p \leq 50$ kpc within ~ 8 Gyr in the model T9 with $M_{dm,l} = 3 \times 10^{10} M_{\odot}$ ($F_{m,gr} = 0.03$) owing to inefficient dynamical friction of the less massive LMC. This result implies that if the Galaxy was already as massive as $M_{dm,mw} = 10^{12} M_{\odot}$ at the epoch of the LMC accretion onto the Galaxy, then the LMC should have a mass significantly larger than the present mass ($[1 - 2] \times 10^{10} M_{\odot}$) at its accretion epoch in order to reach $R = 50$ kpc in the subsequent orbital evolution. If the Galaxy has a lower mass of $5 \times 10^{11} M_{\odot}$, then the LMC with $M_{dm,l} = 3 \times 10^{10} M_{\odot}$ can show $R_p \leq 50$ kpc in the model T21. This result implies that if the LMC has a lower original mass ($M_{dm,l} \sim 3 \times 10^{10} M_{\odot}$), then the Galaxy should have a lower mass at the epoch of the LMC accretion for the LMC to finally reach $R = 50$ kpc. Therefore the results of the models T9 and T21 suggest that the present location and orbit of the LMC can give constraints on the

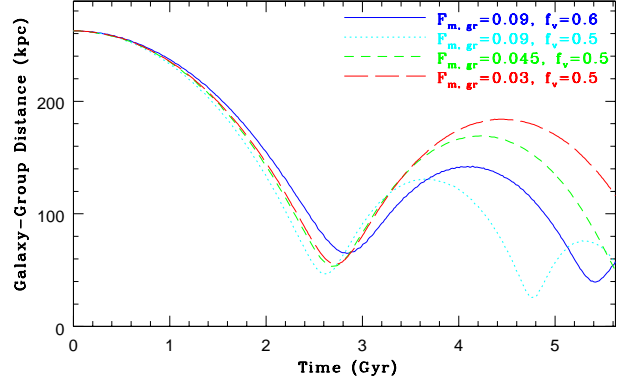


Figure B1. The time evolution of the distance between a disk galaxy and a group infalling onto the galaxy for the last 5.6 Gyr in four different models with $F_{m,gr} = 0.09$ and $f_v = 0.6$ (blue solid), $F_{m,gr} = 0.09$ and $f_v = 0.5$ (cyan dotted), $F_{m,gr} = 0.045$ and $f_v = 0.5$ (green short-dashed), and $F_{m,gr} = 0.03$ and $f_v = 0.5$ (red long-dashed). For these models, $\theta = 60^\circ$.

original mass of the LMC and the Galaxy mass at the LMC accretion.

The LMC in the model T14 with $M_{dm,l} = 6 \times 10^{11} M_{\odot}$ ($F_{m,gr} = 0.06$), $f_{v,t} = 0.7$, and $f_{v,r} = 0.2$ can not reach $R = 50$ kpc within ~ 8 Gyr, though the LMC in the model T4 with $M_{dm,l} = 9 \times 10^{11} M_{\odot}$ ($F_{m,gr} = 0.09$) and the same $f_{v,t}$ and $f_{v,r}$ can reach $R = 50$ kpc within ~ 6 Gyr. This result suggests that the LMC with a lower mass needs to have lower $f_{v,t}$ (for a fixed $f_{v,r}$) to reach $R = 50$ kpc within ~ 8 Gyr. The models with higher $f_{v,t}$ (> 0.7) and higher $f_{v,r}$ (> 1) do not show $R_p \leq 50$ kpc for the LMC. For example, the orbit of the LMC shows the pericenter of more than 100 kpc and the apocenter much larger than the virial radius of the Galaxy in the model T8 with $f_{v,t} = 0.9$ and $f_{v,r} = 1.0$. These results in Fig. A1 clearly demonstrate that there is a required range of model parameters for the LMC to finally reach $R = 50$ kpc since the LMC accretion onto the Galaxy from outside of the Galactic virial radius.

APPENDIX B: THE GALACTIC PRECESSION DUE TO ACCRETION OF SMALL GROUPS AND SATELLITE GALAXIES

Recent high-resolution cosmological simulations of the formation of a Milky Way-like halo in a Λ cold dark matter cosmology have shown that a significant fraction of the sub-halos have been accreted in group (e.g., Li & Helmi 2008). Since the orbital parameters of the groups accreting onto the Galaxy can be significantly different from those of the LMC (or the LMC group), it is worthwhile for the present study to briefly discuss how group infall can influence the dynamical evolution of the Galaxy for different orbital parameters of the groups. Here we focus on how θ_d depends on (i) $F_{m,gr}$ (i.e., the mass ratio of a group to the Galaxy) and (ii) θ_{gr} , which is the inclination angle between the orbital plane of a group and the x - y plane.

Fig. B1 shows the orbital evolution of a group in the Galaxy for models with different $F_{m,gr}$ and f_v for the last 5.6 Gyr. Owing to dynamical friction of the group against the dark matter halo of the Galaxy, the pericenter distance

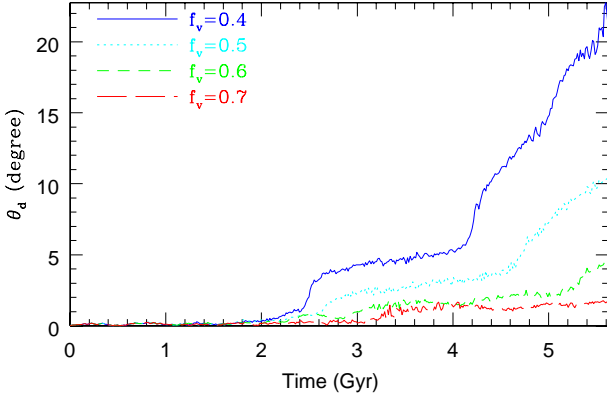


Figure B2. The time evolution of the angle (θ_d) between the z -axis and the orientation of the rotation axis of a stellar disk in four different models with $f_v = 0.4$ (blue solid), $f_v = 0.5$ (cyan dotted), $f_v = 0.6$ (green short-dashed), and $f_v = 0.7$ (red long-dashed). For these models, $F_{m,gr} = 0.09$ and $\theta_{gr} = 60^\circ$.

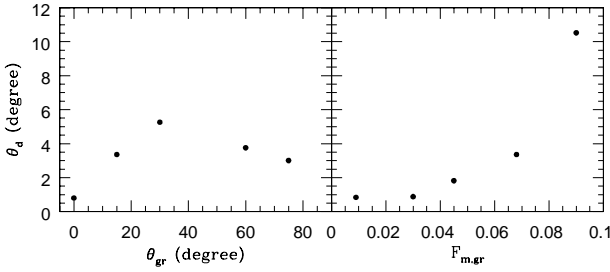


Figure B3. The dependences of θ_d on θ_{gr} (left) and $F_{m,gr}$ (right). The models in the left panel have $F_{m,gr} = 0.09$ and $f_v = 0.6$ whereas those in the right panel have $f_v = 0.5$ and $\theta_{gr} = 60^\circ$.

($R_{p,gr}$) of the orbit becomes progressively smaller as the group moves around the disk: $R_{p,gr}$ for the first and second pericenter passages are 46.6 kpc and 33.7 kpc, respectively, in the model with $F_{m,gr} = 0.09$ and $f_v = 0.5$. The final $R_{p,gr}$ depends on $F_{m,gr}$ and f_v such that (i) $R_{p,gr}$ is larger in models with larger f_v for a given $F_{m,gr}$ and (ii) it is larger for smaller $F_{m,gr}$ for a given f_v . Therefore the disk galaxy can more strongly feel the time-changing tidal torque from the infalling group in models with smaller f_v and larger $F_{m,gr}$ so that the stellar disk can be strongly influenced by the group infall in these models.

Fig. B2 shows that θ_d of the stellar disk in each of the models with the same $F_{m,gr}$ yet different f_v becomes larger as galaxy-group interaction proceeds during group infall. The time evolution of θ_d is more dramatic in the models with smaller f_v owing to smaller $R_{p,gr}$ thus stronger tidal torque of groups. The final θ_d in the models with $f_v = 0.4, 0.5, 0.6$, and 0.7 are $22.7^\circ, 10.5^\circ, 4.5^\circ$, and 1.8° , respectively: galactic precession (pole shift) is more remarkable in the models with smaller f_v . The rate of the precession ($\dot{\theta}_d$) in the last 1 Gyr ($T = 4.6 - 5.6$ Gyr) is also larger in the models with smaller f_v : $\dot{\theta}_d$ in the models with $f_v = 0.4, 0.5, 0.6$, and 0.7 are 8.9, 6.0, 2.3, and 0.6 degrees Gyr^{-1} , respectively. In comparison with almost steady increase of θ_d for the last 1 Gyr, the time evolution of ϕ_d is much less steady in all models of the present study. As discussed later, the

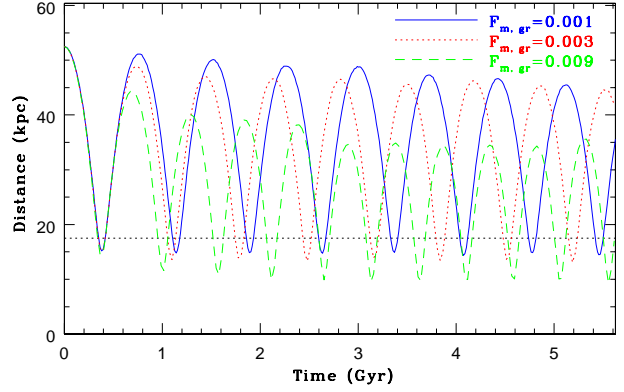


Figure B4. The time evolution of distance between a disk galaxy and an infalling group (including a dwarf) for three different models with $F_{m,gr} = 0.001$ (blue solid), 0.003 (red dotted), and 0.009 (green short-dashed). For these models, $f_v = 0.5$ and $\theta_{gr} = 60^\circ$. The size of the stellar disk is shown by a black dotted line for comparison.

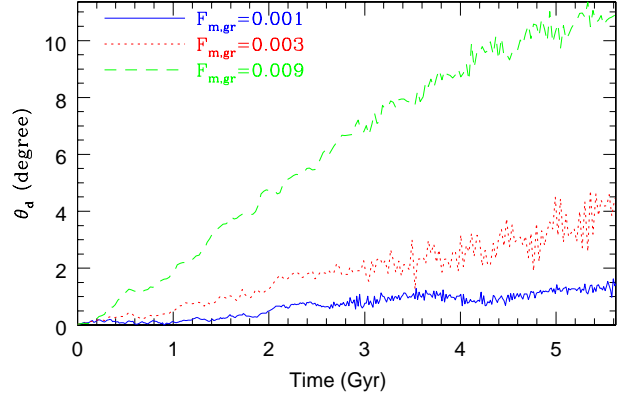


Figure B5. The time evolution of θ_d of a disk galaxy for three different models shown in Figure 8.

higher rates in the models with $f_v \leq 0.6$ (an order of $10\mu\text{as yr}^{-1}$) can be detected by future astrometry satellites with μas precision like GAIA.

As the present study has shown, if the *initial* total mass of a satellite galaxy including the extended massive dark matter halo is as large as 0.3% of the total mass of its host galaxy and if the pericenter distance of its orbit around the host is as small as R_d (=disk size), then the satellite can cause an appreciable amount of the galactic precession ($\theta_d \approx 4^\circ$ and $\dot{\theta}_d \approx 1^\circ \text{Gyr}^{-1}$). If we assume that the total mass of the Galaxy is $10^{12}M_\odot$ (which is consistent with the observationally inferred value by Wilkinson & Evans 1999), then the total mass of Sgr (M_{Sgr}) and the pericenter distance of the Sgr's orbit ($R_{p,\text{Sgr}}$) need to be at least $3 \times 10^9 M_\odot$ and less than ~ 18 kpc, respectively, for Sgr to cause the Galactic precession with the rate of $\dot{\theta}_d \approx 1^\circ \text{Gyr}^{-1}$.

As shown in Fig. B3, the comparative model with $\theta_{gr} = 0^\circ$ shows very small final θ_d (0.8°), which means that the orbit of a group infalling onto a galaxy needs to be inclined to some extent with respect to the stellar disk so as to cause the precession of the disk. The models with smaller $F_{m,gr}$ for a given f_v show smaller final θ_d owing to weaker tidal perturbation from infalling groups. The two models

with $f_v = 0.6$ and -0.6 show similar final θ_d ($\approx 4.5^\circ$) yet appreciably different final ϕ_d ($\phi_d = 86^\circ$ and 76° , respectively), which indicates that the direction of the orbital angular momentum of a group infalling onto a galaxy is also important for the final orientation of the rotation axis of the disk.

The present models with small $F_{m,gr}$ (< 0.01) do not show any significant changes in physical properties of the stellar disk during and after group infall, if the groups are accreted on the disk galaxy from outside the virial radius of the galaxy (thus with large $R_{p,gr}$). Such small groups may well be able to influence the stellar disk if $R_{p,gr}$ is as small as the disk size of the galaxy (R_d). We have investigated the models with $F_{m,gr} < 0.01$, $R_i = 3R_d$, and $f_v = 0.5$ in order to discuss whether some of the Galactic satellite galaxies close to the Galactic disk can cause the Galactic precession and pole shift. In these models, the most of the dark matter halo of infalling groups can be rapidly and efficiently stripped by the strong tidal field of the disk galaxy. Therefore, the central dwarf galaxies embedded in the original cores of dark matter halos of their host groups can influence the stellar disk in these models.

Fig. B4 shows that although more massive groups can reach closer to the stellar disk owing to more effective dynamical friction, the differences in $R_{p,gr}$ between the three models are not so remarkable. As a result of $R_{p,gr}$ being smaller than R_d , the galaxy-group (or galaxy-dwarf) interaction can dynamically influence the stellar disk. Fig. B5 shows that if $F_{m,gr} \geq 0.003$, then the final θ_d can be larger than 4° (which is as large as that derived in the standard model with much larger $F_{m,gr}$). The final θ_d is larger for larger $F_{m,gr}$ owing to stronger tidal perturbation of galaxy-group interaction and this dependence can be seen in other models with different f_v and θ_d . It should be stressed that although the model with $F_{m,gr} = 0.009$ shows a large θ_d at $T = 5.6$ Gyr, the central dwarf galaxy has not yet merged with the disk galaxy.

Recent dynamical models of Sgr that can explain the observed physical properties of the stellar streams associated with Sgr have shown that $M_{Sgr} = 6.4^{+3.6}_{-2.4} \times 10^8 M_\odot$ and $R_{p,Sgr} \approx 15$ kpc (See Figure 7 in Law & Majewski 2010). Therefore, it seems that the original bound stellar mass estimated by Law & Majewski (2010) is well below the required mass of Sgr that can cause the Galactic precession. However the above mass estimation does not include the total mass of the dark matter halo which Sgr initially had when Sgr first passed by the Galaxy. If Sgr initially had the dark matter halo with the total mass being more than ten times larger than that of the baryonic component, then M_{Sgr} can be much larger than the required mass ($= 3 \times 10^9 M_\odot$) for the Galactic precession. Thus, although the present Sgr is unlikely to cause the precession, it might have caused the pole shift when it first passed by the Galaxy.

APPENDIX C: THE DISTRIBUTION OF STRIPPED LMC HALO STARS

Bekki (2011) has recently investigated the distribution of stars stripped from the LMC stellar halo in the Galactic halo and suggested that the structure and kinematics of the stripped LMC stars can have fossil information on the epoch of the LMC accretion onto the Galaxy. However, the

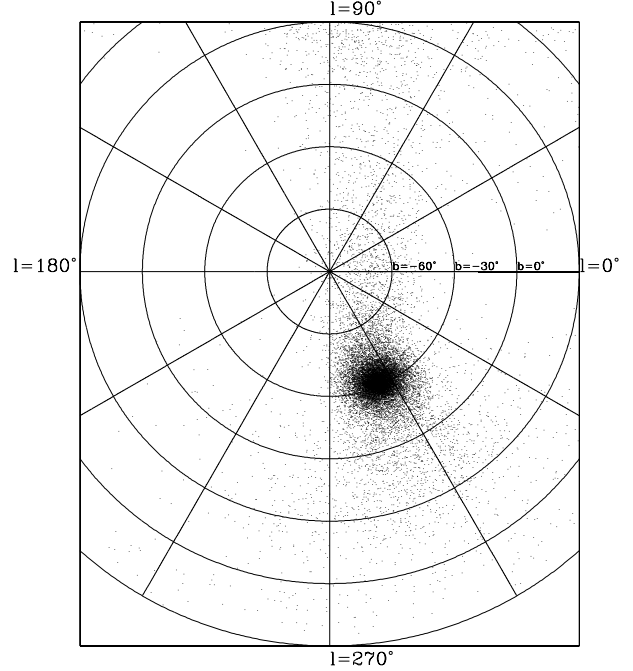


Figure C1. The distribution of the stripped LMC stellar halo stars in the Galactic coordinate for the standard model.

present position of the LMC was not reproduced well by Bekki (2011). Therefore the simulated 3D distribution of the stripped LMC halo stars can not be directly compared with the observed one that will be derived by future observational studies. We thus adopt the same LMC stellar halo model as that in Bekki (2011) and thereby investigate the distribution of the stripped LMC halo stars in the Galaxy.

Fig. C1 shows the distribution of the stripped LMC halo stars projected onto the Galactic coordinate (l, b) in the standard model T1. Although the stripped stars are located in the region where the Magellanic Stream exists, they do not form a narrow tidal stream there. The LMC halo extends to the SMC region and seems to be like a common halo that includes the LMC and the SMC. The predicted physical properties (e.g., locations and radial velocities) of the stripped LMC halo stars can be used for detecting the stars by SkyMapper telescope (Keller et al. 2007).